International Atomic Energy Agency

INDC(NDS)-255

INDC INTERNATIONAL NUCLEAR DATA COMMITTEE

RADIATIVE LOSSES AND ELECTRON COOLING RATES FOR CARBON AND OXYGEN PLASMA IMPURITIES

R. Marchand*, R.K. Janev, and X. Bonnin*

International Atomic Energy Agency, P.O. Box 100

A-1400 Vienna, Austria

January 1992

* INRS-Energie, C.P. 1020, Varennes QC, J3X 1S2, Canada

INDC(NDS)-255

RADIATIVE LOSSES AND ELECTRON COOLING RATES FOR CARBON AND OXYGEN PLASMA IMPURITIES

R. Marchand*, R.K. Janev, and X. Bonnin*

International Atomic Energy Agency, P.O. Box 100

A-1400 Vienna, Austria

January 1992

* INRS-Energie, C.P. 1020, Varennes QC, J3X 1S2, Canada

Abstract

Radiative losses and electron cooling rates are calculated for carbon and oxygen ions under conditions relevant to fusion plasmas. Both rates are calculated with the most recent recommended atomic data. A modified coronal model which includes the effects of metastable states is described and used to calculate the rates. Comparisons with other approaches are also discussed.

Reproduced by the IAEA in Austria
January 1992

92-00376

1. Introduction

Radiative losses are known to contribute a large fraction of the total energy losses in present tokamaks. It is estimated that they should also be critical in future reactors. For example, line radiation by light impurities in the edge region could help distribute the exhausted power over a larger area of the neutralizer plates and, thus, alleviate the erosion problem in the divertor. The presence of heavy impurities in the core will always be detrimental. In addition to diluting the fuel there, strong line radiation by non fully stripped ions will make the conditions required for ignition more difficult to achieve. With the design of the next generation machines (ITER and NET) entering its final phase, it is important that the plasma transport models used in this design be equipped with the best available atomic rates. These considerations have recently stimulated much interest in the construction of models and data bases required for the calculation of atomic-related energy loss rates. These models range in complexity from the simple average-ion approach with semi-empirical rates (Post, et al. 1977), to detailed calculations using recommended data (Summers and McWhirter 1979, Summers and Hooper 1983, McWhirter and Summers 1984 Keane and Skinner 1986). Although the formalism required for an accurate calculation of the rates has been well established, the effort for computing such rates is still very much in progress. This evolution is tied to the completeness in the atomic data at any given time, and to the continuing efforts to add new and more accurate data to the existing data bases.

The primary objective of this report is to present calculations of the radiative losses and electron cooling rates, based on the latest recommended data for carbon and oxygen ions. A method is proposed to account for metastable states in the temperature and density range of

interest to tokamak plasmas. This method is used to estimate the importance of metastable states on the rates. Finally, the completeness of the recommended excitation rates used in the calculations is assessed by comparing results obtained with and without semi-empirical rates for transitions to highly excited states, for which recommended data is not available.

2. Models and basic equations for radiative and electron-energy losses.

2.1 Energy balance.

Radiative losses and electron cooling rates are of interest because they enter energy balance equations. The general form of an energy balance equation is

$$\frac{\partial U}{\partial t} + \nabla\cdot\vec{Q} + \nabla\cdot(P\cdot\vec{v}) = S \qquad (1)$$

where U represents an energy density, $\vec{Q}$ is the associated energy flux, P is a pressure tensor, and S represents an external source (positive) or sink (negative) of energy. The distinction between radiative losses and electron cooling rates is related to the different kind of energy density that is considered. The radiative power loss is required when considering the total energy density. Electron cooling rates, on the other hand, are required when considering the electron energy density. This is explained in more detail below.

a) Total energy balance.

In this case, U is the sum of thermal, kinetic, and chemical energy densities for all species in the plasma; that is

$$U = \sum_j \left\{ n_j T_j + n_j \frac{1}{2} M_j v_j^2 + n_j \mu^j \right\} \qquad (2)$$

where, for a given species j, n_j is the density of particles, T_j is the temperature, M_j is the mass of a particle, v_j is the average or macroscopic velocity, and μ^j is the chemical potential. For simplicity, in the following, we assume a single element of nuclear charge Z and possible ionisation stages from neutral to fully ionized. These are identified by indices i ranging respectively from 0 to Z. The chemical potential is defined by

$$\mu^i = \mu_0^i + \langle\varepsilon^i\rangle \tag{3}$$

where $\langle\varepsilon^i\rangle$ is the average excitation energy of ionisation stage i, and where the coronal potential μ_0^i is defined recursively by

$$\mu_0^i = \mu_0^{i-1} + \varepsilon_0^{i-1} \tag{4}$$

with $\mu_0^0=0$ and ε_0^i being the ground state ionisation energy for stage i. The energy source term in this case is the sum of all external sources, minus all energy loss rates. Symbolically,

$$S = S_{tot\text{-}in} - P_r \tag{5}$$

where $S_{tot\text{-}in}$ would include such terms as ohmic and neutral beam heating. P_r represents the total power lost by radiation, per unit volume.

b) Electron cooling rates.

When modelling transport in a tokamak plasma, it is customary to consider the thermal plus kinetic energy densities for individual species, or for collections of species. For example, the B2 code presently used to support the design of ITER (Braams 1987) solves for the electron thermal energy and for ion thermal energy separately. When considering the electron thermal energy (the electron kinetic energy is

negligible), the source term appearing in the right hand side of Eq. (1) has the following general form

$$S = S_{el-in} + S_{e-ion} - P_e \qquad (6)$$

where S_{el-in} represents the source of outside energy directly delivered to the electrons. This term would include, for example, ohmic heating. S_{e-ion} is the rate at which energy is transferred from the ions to the electrons by Coulomb collisions and P_e is the electron cooling rate specifically related to atomic processes.

2.2 Structure and general properties of the loss terms.

The radiative power loss P_r, which represents the rate at which energy is lost by radiation per unit plasma volume, consists of the following contributions:

- line radiation associated with the radiative cascade which follows collisional excitation, radiative and dielectronic recombination,
- continuum radiation associated with radiative recombination, and
- bremsstrahlung.

We note that for the densities of interest to tokamak plasmas, three body recombination is negligible. This process is therefore not taken into account in the calculations given below.

The electron cooling rate P_e accounts for the following contributions:

- collisional excitation,
- ionisation,
- radiative and dielectronic recombination, and
- bremsstrahlung.

A precise definition of these contributions depends on the level at which the atomic physics is modelled. Detailed expressions are given in

the next section. At this stage, it is instructive to look at some general properties of P_r and P_e. These are:

a) $P_r < P_e$ when the plasma is in an ionizing regime.

Indeed, when the distribution of ionisation stages shifts towards larger ionisation, the chemical energy of the ions increases. Ionisation requires an additional expenditure of electron energy, which does not result in radiation.

b) $P_r > P_e$ when the plasma is in a recombining regime.

In the opposite case, when the distribution of ionisation stages shifts towards lower ionisation, the chemical energy of the ions decreases and radiative losses exceed electron thermal losses. Phenomenologically, an

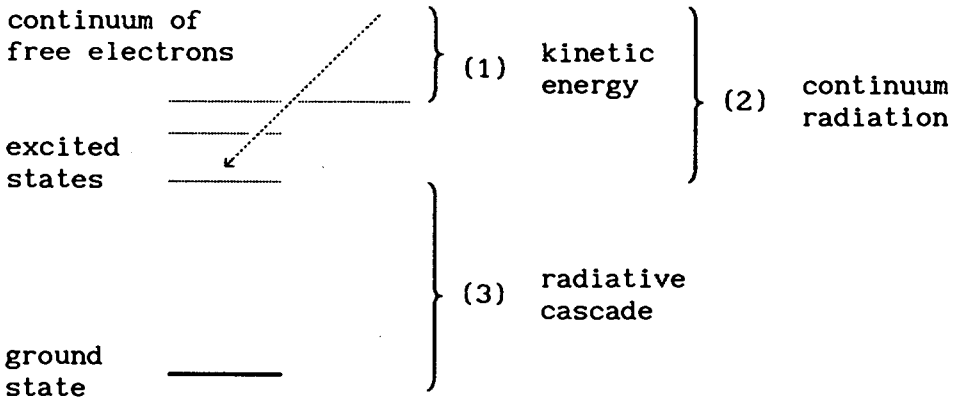

Fig. 1. Illustration of the various contributions to P_r (2 and 3) and P_e (1) associated with radiative recombination.

electron which recombines only contributes its kinetic energy to P_e (contribution 1 in Fig. 1). For P_r, however, it contributes its kinetic energy plus the ionisation energy of the recombined ion (contributions 2 and 3 in Fig. 1). The various contributions to P_r and P_e associated with radiative recombination are illustrated in Fig. 1.

c) $P_r = P_e$ when the plasma is at steady ionisation balance.

Considering that the chemical energy density is constant at steady state, this statement is obvious from conservation of energy.

2.3 Methods of calculation.

We now give explicit expressions for the radiative loss and electron cooling rates, in connection with various levels of approximation for the atomic physics. These are: 1) the average ion model, 2) the detailed configuration coronal model, and 3) the collisional-radiative model. In part 4), we propose a method of calculation for the rates in a modified coronal model which accounts for metastable states.

2.3.1 Average-ion model.

One of the simplest descriptions of atomic processes consists of approximating the distribution of ionisation stages for a given impurity species by a single ion with a (fractional) charge which represents the average impurity charge stage. This is the so-called average-ion model (Strômgren 1932, Chandrasekar 1939, Lokke, et al. 1977). It is customary in this approach to calculate the ion energies in the screened hydrogenic approximation (More 1982, Marchand, et al. 1990), with a possible allowance for a single $\Delta n=0$ transition in the valence shell (Post, et al. 1977). Also, for simplicity, the atomic rates are often calculated from semi-empirical formulae. The state of such an ion is entirely determined by the populations P_n of the various energy levels n. With the definitions given in table 1, the expressions for P_r and P_e, for a density n_Z of impurity species Z, are:

$$P_r = n_Z\left\{ \sum_{mn} P_m A^q_{mn} Q_n \varepsilon^q_{nm} + \sum_n \int d^3v \left(\tfrac{1}{2}Mv^2+\varepsilon^q_n\right) v\sigma^{q-1}_{rr,n}(v) Q_n f(\vec{v}) + B^q \right\} \quad (7)$$

and

$$P_e = n_Z\left\{ \sum_{nm} P_n X^q_{nm} Q_m \varepsilon^q_{nm} + \sum_n P_n S^q_n \varepsilon^q_n + \sum_n \int d^3v \, \tfrac{1}{2}Mv^2 v\sigma^{q-1}_{rr,n}(v) Q_n f(\vec{v}) \right.$$
$$\left. + \sum_{lnm} P_l \int d^3v \, \tfrac{1}{2}Mv^2 v\sigma^{q-1}_{dr,lnm}(v) Q_n f(\vec{v}) + B^q \right\}, \quad (8)$$

Table 1. Definition of the variables and rates used in the average ion approximation.

A^q_{mn}	Transition probability for transition m → n in ion of charge q.
B^q	Power radiated by bremsstrahlung per unit volume, per unit ion of charge q.
P_n	Number of electrons in energy level n.
Q_n	$1-P_n$/(maximum number of electrons allowed in level n).
S^q_n	Ionisation rate from level n in ion of charge q.
X^q_{nm}	Excitation rate for transition n → m in ion of charge q.
ε^q_n	Ionisation energy from level n in ion of charge q.
ε^q_{nm}	Excitation energy for transition n → m in ion of charge q.
$\sigma^{q-1}_{rr,n}$	Cross section for radiative recombination on level n, in ion with initial charge q.
$\sigma^{q-1}_{dr,lnm}$	Cross section for dielectronic recombination on level m, accompanied with an excitation from level l to n. The charge of the ion before recombination is q.

N.B.: Subscript 0 refers to the ground state.

where $f(\vec{v})$ is the electron distribution function. These expressions are general and they are valid, in particular, when multistep processes are taken into account. In the special case of a very low plasma density, the coronal approximation may be made, and the first term in Eq. (7) is more conveniently written as

$$\sum_{mn} P_m A^q_{mn} Q_n \varepsilon_{nm} = \sum_{nm} P_n X^q_{nm} Q_m \varepsilon^q_{nm} + \sum_n \int d^3v \; v\sigma^{q-1}_{rr,n}(v) Q_n f(\vec{v}) \varepsilon^q_{0n}$$

$$+ \sum_{nm} \int d^3v \; v\sigma^{q-1}_{dr,0nm}(v) Q_n f(\vec{v}) (\varepsilon^q_{0n} + \varepsilon^q_{0m}). \qquad (9)$$

2.3.2 Detailed configuration coronal model.

An obvious improvement over the average ion model consists of accounting for all possible ionisation stages explicitly. Radiative losses and electron cooling rates are then calculated by summing their respective contributions over all ionisation stages. If, as in most earlier calculations of radiative losses, the plasma is assumed to be coronal, the expressions for the rates are

$$P_r = \sum_i n_i \Bigg\{ \sum_\alpha X^i_{0\alpha}\varepsilon^i_{0\alpha} + \sum_\alpha \int d^3v \left(\tfrac{1}{2}Mv^2+\varepsilon_0^{i-1}-\varepsilon_{0\alpha}^{i-1}\right) v\sigma^{i-1}_{rr,0\alpha}(v) f(\vec{v}) + \sum_\alpha R^{i-1}_{0\alpha}\varepsilon^{i-1}_{0\alpha} + \sum_{\alpha\beta} D^{i-1}_{0\alpha\beta}(\varepsilon^i_{0\alpha}+\varepsilon_0^{i-1}) + B^i \Bigg\}, \tag{10}$$

and

$$P_e = \sum_i n_i \Bigg\{ \sum_\alpha X^i_{0\alpha}\varepsilon^i_{0\alpha} + S^i_0\varepsilon^i_0 + \sum_\alpha \int d^3v \, \tfrac{1}{2}Mv^2 v\sigma^{i-1}_{rr,0\alpha}(v) f(\vec{v}) + \sum_{\alpha\beta} \int d^3v \, \tfrac{1}{2}Mv^2 v\sigma^{i-1}_{dr,0\alpha\beta}(v) f(\vec{v}) + B^i \Bigg\} \tag{11}$$

where n_i is the density of ionisation stage i,

$$R^{i-1}_{0\alpha} = \int d^3v \; v\sigma^{i-1}_{rr,0\alpha}(v) f(\vec{v}) \tag{12}$$

is the rate of radiative recombination to state α in ionisation stage i-1 from ionisation stage i initially in its ground state, and

$$D^{i-1}_{0\alpha\beta} = \int d^3v \; v\sigma^{i-1}_{dr,0\alpha\beta}(v) f(\vec{v}) \tag{13}$$

is the rate of dielectronic recombination in Rydberg state β accompanied by the excitation of a core electron from the ground state to state α. The radiative loss term in Eq. (10) is very similar in form to Eq. (1) of Summers and McWhirter (1979). In their terminology, $P_r/(n_e\sum n_{i\alpha})$ is

the radiative power loss function while the term in curly brackets in Eq. (11) divided by the electron density is the radiative power loss coefficient.

2.3.3 Full collisional radiative calculation.

A further improvement in the atomic physics would include multistep processes such as ionisation and (de)excitation from excited states. This is particularly interesting when one considers ions with long-lived metastable states. Approaches to account for multistep processes have been described, for example, by Bates, et al. (1962), by Summers (1977), and by Summers and Hooper (1983). We shall not discuss these approaches here. We assume, instead, that the density $n_{i\alpha}$ of ionisation stage i in state α has somehow been calculated, and proceed with general expressions for the radiative and electron cooling rates. With the definitions given in Table 2, these are

$$P_r = \sum_i \left\{ \sum_{\beta\alpha} n_{i\alpha} A^i_{\beta\alpha} \varepsilon^i_{\alpha\beta} + \sum_{\alpha\beta} n_{i\alpha} \int d^3v \left(\tfrac{1}{2}Mv^2 + \mu^i_\alpha - \mu^{i-1}_\beta\right) v\sigma^{i-1}_{rr,\alpha\beta}(v) f(\vec{v}) \right.$$

$$\left. + \sum_\alpha n_{i\alpha} B^i_\alpha \right\}, \qquad (14)$$

and

$$P_e = \sum_i \left\{ \sum_{\alpha\beta} n_{i\alpha} X^i_{\alpha\beta} \varepsilon^i_{\alpha\beta} + \sum_\alpha n_{i\alpha} S^i_\alpha \varepsilon^i_\alpha + \sum_{\alpha\beta} n_{i\alpha} \int d^3v \, \tfrac{1}{2}Mv^2 v\sigma^{i-1}_{rr,\alpha\beta}(v) f(\vec{v}) \right.$$

$$\left. + \sum_{\alpha\beta\delta} n_{i\alpha} \int d^3v \, \tfrac{1}{2}Mv^2 v\sigma^{i-1}_{dr,\alpha\beta\delta}(v) f(\vec{v}) + \sum_\alpha n_{i\alpha} B^i_\alpha \right\}, \qquad (15)$$

where $\mu^i_\alpha = \mu^i_0 + \varepsilon^i_{0\alpha}$. The chemical potential of stage i in its ground state μ^i_0, is defined in paragraph 2.1a.

Table 2. Definition of the variables and rates entering the general definition of the energy loss rates in Eqs. (14) and (15).

$n_{i\alpha}$	Density of ions in the ionisation stage i and in state α.
μ_{α}^{i}	Chemical potential of ions in ionisation stage i and state α.
$\sigma_{rr,\alpha\beta}^{i-1}$	Cross section for radiative recombination into state β of ionisation stage i-1, from state α of ionisation stage i.
$\sigma_{dr,\alpha\beta\delta}^{i-1}$	Cross section for dielectronic recombination in Rydberg state δ of the recombined ion stage i-1, accompanied with a core excitation from state α to β.

2.3.4 Modified coronal model, with metastable state effects.

In Sec. 4 we present results obtained in a modified coronal approximation, which accounts for long-lived metastable states. For simplicity, the following assumptions are made:

1 - There are long-lived metastable states for which the largest transition probability is smaller than, or comparable to the largest collisional rate to the ground or to other metastable states. In the following, all excited states which cannot decay radiatively to a lower energy state via an optically allowed transition will be treated as long-lived metastables.

2 - For metastable states, the relative densities $n_{i\alpha}$ for a given ionisation stage i are determined by:

- collisional (de)excitation between the ground and metastable states,
- possible radiative decay,
- ionisation from the ground and metastable states, and
- excitation from the ground and metastable states, to non

metastable states, followed by radiative cascade back to the ground or metastable states.

3 - Multistep processes are neglected for excited non metastable states.

4 - Recombination, whether radiative or dielectronic, may take place from metastable states. When the recombined ion is in an excited state, it decays instantaneously to its ground state.

We note that in this model, the relative populations $n_{i\alpha}$ of the ground and metastable states of a given ionisation stage i are not affected by recombination from the upper ionisation stage, or by the different rates at which recombination takes place from the different states α of stage i. This assumption is justified by the fact that recombination is generally a slow process. Our calculations using that model will be valid provided that P_r is dominated by excitation, and that P_e is dominated by excitation plus ionisation. These conditions will have to be verified a posteriori. The expression for P_r in this approximation is

$$P_r = \sum_i \Big\{ \sum_{\beta\alpha} n_{i\beta} A^i_{\beta\alpha} \varepsilon^i_{\alpha\beta} + \sum_{\alpha\beta\delta} n_{i\alpha} \int d^3v \; \varepsilon^{i-1}_{\beta} v \sigma^{i-1}_{dr,\alpha\beta\delta}(v) f(\vec{v})$$

$$+ \sum_{\alpha\beta} n_{i\alpha} \int d^3v \; \left(\tfrac{1}{2}Mv^2 + \varepsilon^i_{0\alpha} - \varepsilon^{i-1}_0\right) v \sigma^{i-1}_{rr,\alpha\beta}(v) f(\vec{v}) + \sum_{\alpha} n_{i\alpha} B^i_{\alpha} \Big\}, \qquad (16)$$

The expression for P_e is the same as given in Eq. (15). Note that in these expressions, the following assumptions are made:

- $X^i_{\alpha\beta} = S^i_{\alpha} = 0$ whenever state α is not identified as the ground or a metastable state,
- $B^i_{\alpha} = B^i$ is independent of α.

The density $n_{i\alpha}$ of states α for a given ionisation stage i is obtained by solving the following set of equations:

$$\frac{dn_{i\alpha}}{dt} = \sum_{\beta} \left[-(A^i_{\alpha\beta} + X^i_{\alpha\beta} + \sum_{\delta} D^{i-1}_{dr,\alpha\beta\delta}) n_{i\alpha} + (A^i_{\beta\alpha} + X^i_{\beta\alpha} + \sum_{\delta} D^{i-1}_{dr,\beta\alpha\delta}) n_{i\beta} \right]$$

$$- S^i_{\alpha} n_{i\alpha} + \delta_{0\alpha} \sum_{\beta} S^i_{\alpha} n_{i\alpha} = 0, \qquad (17)$$

with the normalization

$$\sum_{\substack{\text{ground \&} \\ \text{metastables}}} n_{i\alpha} = n_i. \qquad (18)$$

In Eq. (17), the last summation in the left hand side has been introduced to ensure the existence of a non trivial solution. Physically, this term means that the ions lost by ionisation are instantaneously fed back into the ground state. This assumption is somewhat arbitrary. It could have been replaced, for example by

$$\delta_{0\alpha} \sum_{\beta} S^i_{\alpha} n_{i\alpha} \longrightarrow \lambda n_{i\alpha} \qquad (19)$$

which would correspond to a uniform exponential decay $\exp(-\lambda t)$ for all states of ionisation stage i. The exact form of this term should be of little consequence in the final result, provided the rates of excitation $X^i_{\alpha\beta}$ are much larger than the rates of ionisation S^i_{α}.

2.3.5 Steady ionization balance.

It is customary in the calculation of radiative losses, to consider impurities under the so-called steady-state (Post, et al. 1977) or steady-state ionization balance (Summers and Hooper 1979). This condition will also be considered in Sec. 4. A given ion species is at steady ionisation balance when the rate at which any given ionisation stage is lost by ionisation and recombination is exactly balanced by the rate at which it is populated by recombination and ionisation of

neighbouring stages. After some simple algebra, this condition proves to be equivalent to the requirement that the rate at which any stage i ionizes is equal to the rate at which stage i+1 recombines. Considering the model of subsection 2.3.4 for the purpose of the discussion, this is translated mathematically as

$$n_i \sum_\alpha \frac{n_{i\alpha}}{n_i} S^i_\alpha = n_{i+1} \sum_\alpha \frac{n_{i+1\alpha}}{n_{i+1}} \left(\sum_\beta R^i_{rr,\alpha\beta} + \sum_{\beta\delta} D^i_{dr,\alpha\beta\delta} \right) \tag{20}$$

where the densities $n_{i\alpha}$ are determined in terms of the total density n_i of particles in ionisation stage i by Eqs. (17) and (18). This constitutes a set of recursive equations for n_i, which can readily be solved for a given total impurity density.

It is important to stress that steady ionization balance is not implied by a steady-state solution of the plasma transport equation. This has been noted by Hulse (1983) who demonstrated that, because of transport and recycling at the edge, the actual distribution of ionisation stages may differ significantly from that of steady ionisation balance. It is for this reason that atomic loss rates must be known for individual ionisation stages, when modelling tokamak plasmas.

3. Atomic data base.

Whenever possible, we use recommended data for the atomic processes involved in the power loss functions. When recommended data are not available, semi-empirical data are used. In the next paragraphs we briefly review the sources of the data used for excitation, ionisation, radiative and dielectronic recombination, and the transition probabilities. The various quantum states considered in the calculations for carbon and oxygen ions are listed in Appendix A.

3.1 - Excitation.

Most of the excitation rates used in this work are those recommended by Phaneuf, et al. (1987). For certain transitions not considered by these authors, the rates of Itikawa, et al. (1985) have been used. For helium-like ions, the rates recently recommended by Kato, et al. (1989), and for OV, those recommended by Kato, et al. (1990) have been used. For CIV and OVI, the excitation rates from the ground state to the autoionizing states are those of Itikawa, et al. (1987). We note that the cross sections in these references have been fitted over a finite energy interval, with analytic expressions which did not ensure correct extrapolation outside the interval. This circumstance has forced us to construct new fits to the data, for several forbidden transitions in order to extend the rates to higher temperatures. For neutral oxygen, we use the cross sections recently compiled by Laher and Gilmore (1990), and by Itikawa and Ichimura (1990).

For most ionisation stages considered in this calculation, none of the excited states taken into account are autoionizing. The two exceptions are CIV and OVI for which transitions from the ground state to four autoionizing states are considered. In the calculation of the loss terms, the excitation rates to these states are multiplied by the branching ratio for radiative decay. Autoionisation from Auger states is already accounted for in the recommended ionisation cross sections (Lennon, et al. 1988).

Use is made of semi-empirical excitation rates (Post, et al. 1977) for transitions from the ground or metastable states to hydrogenic energy levels with large principal quantum numbers. Specifically, this is used for transitions towards levels $n=n_0+1$, up to $n=10$, where n_0 is the largest principal quantum number of an excited state for which recommended data is available. This use of semi-empirical excitation rates to complement the recommended data will serve to assess the

completeness of those recommended data. This point will be discussed further in Sec. 4.2.2. The excitation rates used for neutral carbon are those of Post, et al. (1977).

3.2 - Ionisation.

Ionisation rates from the ground state are calculated from analytic integration of the cross sections recommended by Lennon, et al. (1988). Ionisation from metastable states is calculated with the Lotz semi-empirical formula (Lotz 1967). Specifically, the cross section from an energy level n containing q_n electrons is assumed to be

$$\sigma_n = aq_n \frac{\ln(E/I_n)}{EI_n} \qquad (21)$$

where $a=4\times10^{-14}cm^2(eV)^2$, E is energy of the incident electron and I_n is the ionisation energy from energy level n.

3.3 - Radiative recombination.

Radiative recombination from the ground state is calculated so as to reproduce recommended total recombination rates. The rates of radiative recombination to specific states are first calculated from approximate scaled hydrogenic formulae. All rates are then multiplied by a constant which is chosen such that the normalized rates correctly reproduce the recommended rate for total radiative recombination. The total recombination rates used are those calculated by Aldrovandi and Péquignot (1973) for all ionisation stages, with the exception of CIII, for which we used the rates calculated by Datz and Dittner (1988). No recommended data has been found for radiative recombination from metastable states. For these, the rates are calculated from scaled hydrogenic expressions.

3.4 - Dielectronic recombination.

As for radiative recombination, the rates of dielectronic recombination are calculated empirically and, when possible, normalized so as to reproduce recommended rates for specific groups of transitions. There are five possibilities for grouping the transitions, corresponding to five possible levels of normalization:

a) total rates, including $\Delta n=0$ (so-called mode B) transitions and $\Delta n>0$ (mode A) transitions,

b) total specific Δn (typically $\Delta n=0$ and $\Delta n=1$) transitions,

c) total $\Delta n>0$ transitions,

d) transition to a specific state, and

e) total transitions to autoionizing states.

Ideally, recommended rates should be used for the various individual transitions possible (case d). When such detailed data are not available, the preferred normalization options are b then c. When that is not available, scaling is done from the total recombination rate (case a). In one instance (recombination from the metastable state of CV), no recommended data have been found and purely semi-empirical rates are used. The level of approximation and the source of the recommended rates are given in Appendix B for all the ionisation stages of carbon and oxygen considered.

The recommended dielectronic recombination rates considered here have been calculated in the zero density limit. At finite densities, the rates are reduced by so-called collisional interruption or thermal equilibration of the Rydberg states with the continuum. Unfortunately, none of the calculations considered offered a simple method to account for this effect. We have accounted for the weak density and temperature dependence of the rates in an ad hoc way, by multiplying the normalized rates by empirical correction factors for $\Delta n\neq0$ and $\Delta n=0$ transitions. Figure 2 shows a comparison between finite density recombination rates

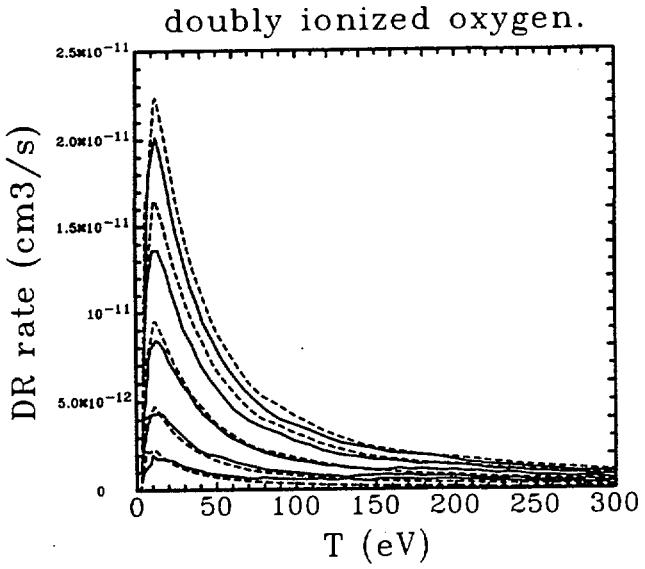

Fig. 2. Comparison between the finite density rates of dielectronic recombination obtained from empirically scaled recommended rates (dashed line) and those calculated by Roszman (solid line) for OIII. The densities considered range from 10^{12} m^{-3} (higher curves) to 10^{20} m^{-3} (lower curves), in increments of 10^{2}.

obtained with this method and those calculated by Roszman (1989) for an OIII ion with inclusion of finite density effects. The generally good agreement suggests that the method adopted here is adequate for the range of plasma densities and temperatures of interest here.

3.5 - Transition probabilities.

Most transition probabilities used in the calculations have been provided by Wiese and Fuhr (1991), and Wiese, et al. (1966). For forbidden transitions in hydrogen and helium-like ions, we use the transition probabilities calculated by Drake (1986, 1971). For helium and beryllium like ions, these are complemented by the transition probabilities of Shevelko, et al. (1989). For beryllium like ions, we also use the transition probabilities of Dufton, et al. (1978).

4. Results.

The results of our calculations are given in Appendix C. They consist of the radiative loss and electron cooling rate coefficients, calculated for every ionisation stage of carbon and oxygen, as a function of temperature. Radiative loss and cooling functions calculated at steady ionisation balance are given in Appendix D. In this section, we concentrate on specific aspects of those results. First, we quantify the effects of metastable states. We then assess the completeness of the recommended data base used to calculate excitation rates. Finally, we make comparisons with other approaches. Unless stated otherwise, all calculations are made with an assumed electron density of $10^{20} m^{-3}$. In the figures, radiative losses and cooling rates are given in units of attowatts m^3. In the past, radiative losses have often been expressed in units of erg s^{-1} cm^3. The conversion between the two units is 1 aW m^3 = 10^{-5} erg s^{-1} cm^3.

4.1 Effect of metastable states.

The effect of metastable states is conveniently illustrated by comparing with results obtained in the usual coronal approximation. We first consider rates for individual charge stages and then, steady ionisation balance.

4.1.1 Comparisons for individual ionisation stages.

Figures 3 and 4 show the internal, or average excitation energy

$$\langle \varepsilon^i \rangle = \sum_\alpha n_{i\alpha} \varepsilon^i_{0\alpha} \Big/ n_i \qquad (22)$$

as a function of temperature calculated for the various charge stages of carbon and oxygen. In these figures, only the charge stages with

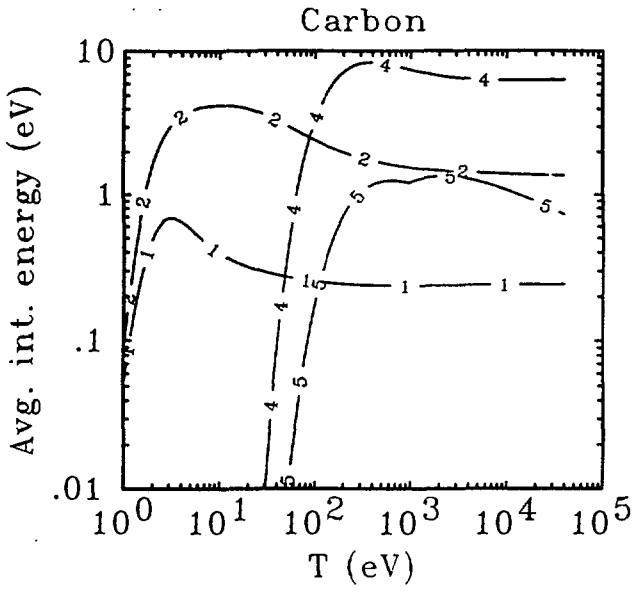

Fig. 3. Average internal energy of the various ionisation stages of carbon which have metastable states, as a function of temperature. The numbers of the curves correspond to the ion charge.

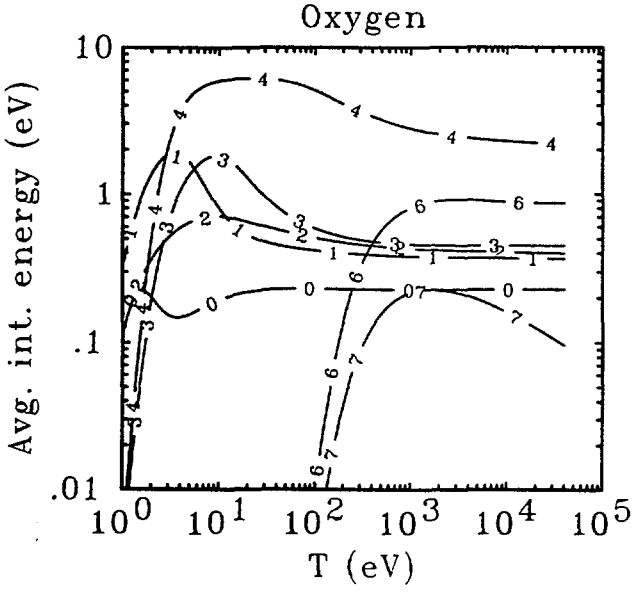

Fig. 4. Average internal energy of the various ionisation stages of oxygen which have metastable states, as a function of temperature.

metastable states are considered. In all cases, the internal energy approaches zero at low temperatures. It reaches a maximum at a temperature comparable to the threshold energy for excitation to a metastable state. At higher temperatures, the internal energies approach finite asymptotic values. The internal energy is a measure of the relative population of the metastable states weighted by the respective threshold energies. We therefore expect metastable states to have a largest effect near temperatures where the internal energy is maximum.

Figures 5 and 6 show the radiative loss coefficients for oxygen and carbon as a function of temperature, computed with (solid line) and without (dashed line) metastable effects. Figures 7 and 8 show the electron cooling rates for the same elements. In these figures, rates are plotted for every ionisation stage, including those (CI, CIV, CVII, OVI, and OIX) with no metastable states. In every case, the effect of metastable states is to either increase or decrease both loss rates simultaneously. Other than that, there is no apparent regularity in the effect of metastables. The largest differences are typically in the temperature range where the internal energy is maximum. The differences there can be of order 30%. We note that for helium and hydrogen-like ions, the results obtained in the low temperature region are nearly independent of metastable states. This is because recombination gives the major contribution to both P_r and P_e at these temperatures and, as stated in Sec. 2.3.4, recombined ions are treated in the coronal approximation.

The ionisation rates computed for every ionisation stage of carbon and oxygen with (solid line) and without (dashed line) metastable effects are plotted in Figs. 9 and 10, respectively. In this case, metastable states are seen to result in an increase of the ionisation rate. The largest increase is again found in the temperature range, where the relative population of metastable states is maximum. The

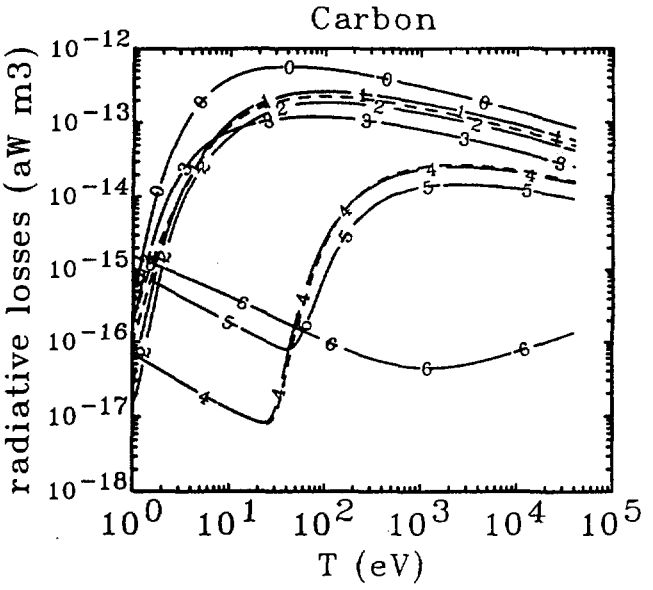

Fig. 5. Radiative loss coefficient for carbon as a function of temperature computed with (solid line) and without (dashed line) metastable effects.

increase in the ionisation rates means that ionisation is facilitated when ions are first excited to a metastable state.

In figures 11 and 12 we show the rate of radiative plus dielectronic recombination computed for every ionisation stage of carbon and oxygen with (solid line) and without (dashed line) metastable effects. With the exception of beryllium like ions, recombination rates are found to be relatively insensitive to the inclusion of metastable states.

We note that, because of its large transition probability, the 2s metastable state in hydrogen-like ions has a negligible effect on the rates at the plasma density considered here. The same remark applies to the singlet 1s2s state in helium ions.

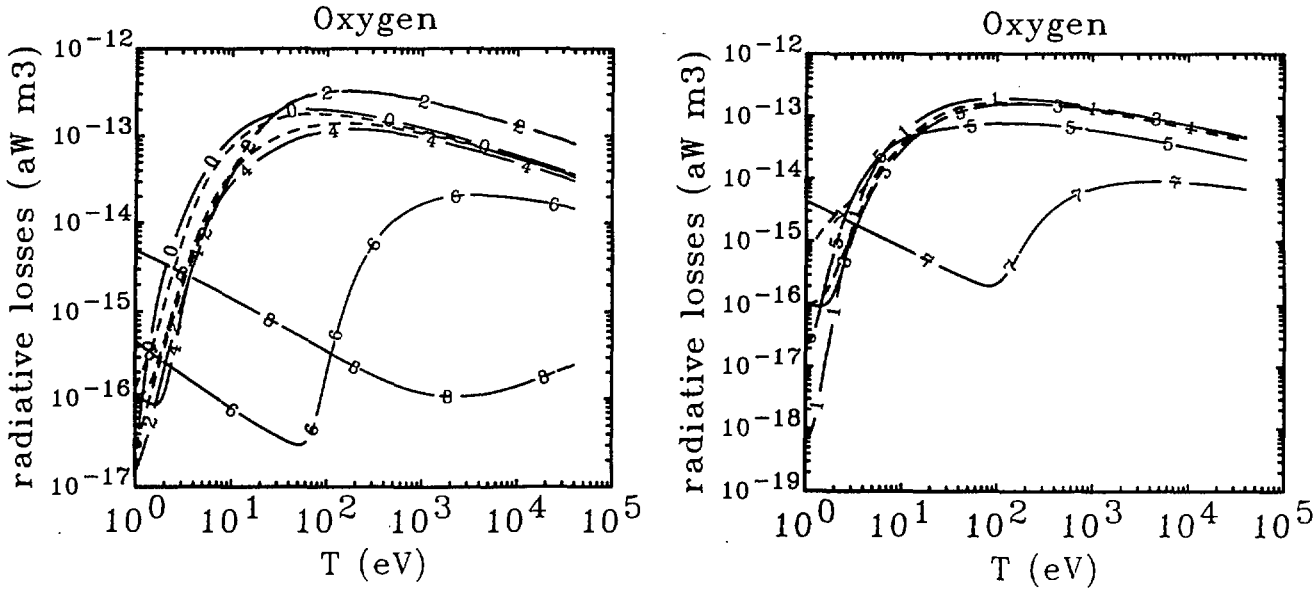

Fig. 6. Radiative loss coefficient for oxygen a function of temperature computed with (solid line) and without (dashed line) metastable effects.

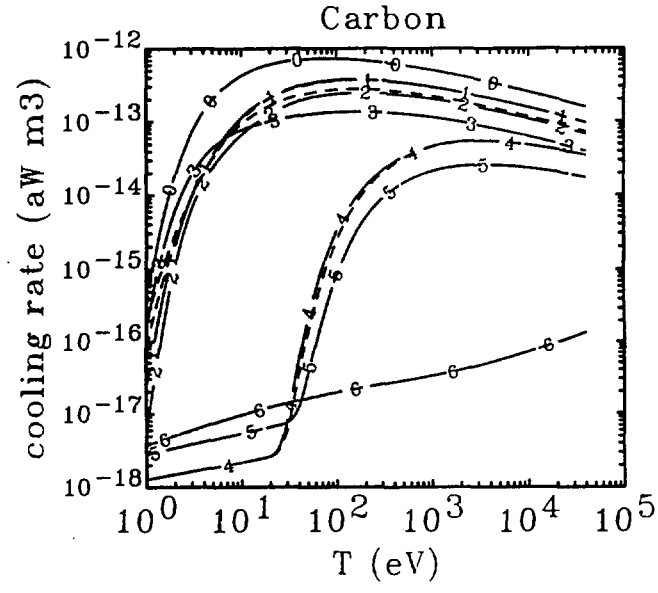

Fig. 7. Electron cooling coefficient for carbon as a function of temperature computed with (solid line) and without (dashed line) metastable effects.

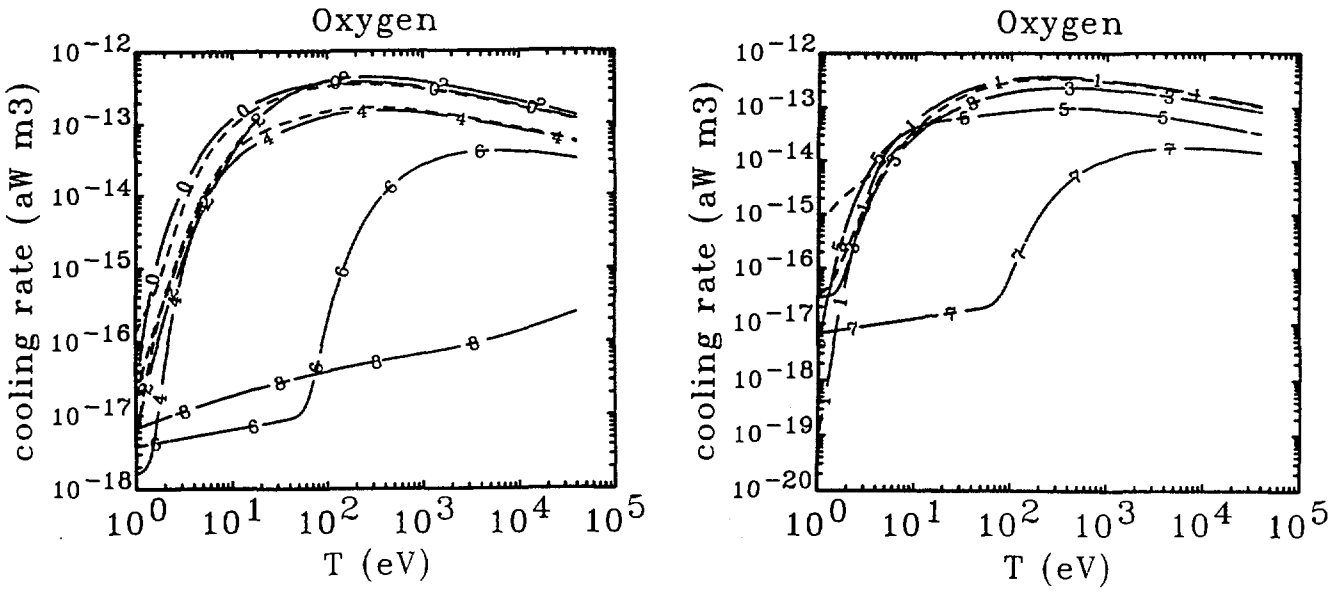

Fig. 8. Electron cooling coefficient for oxygen as a function of temperature computed with (solid line) and without (dashed line) metastable effects.

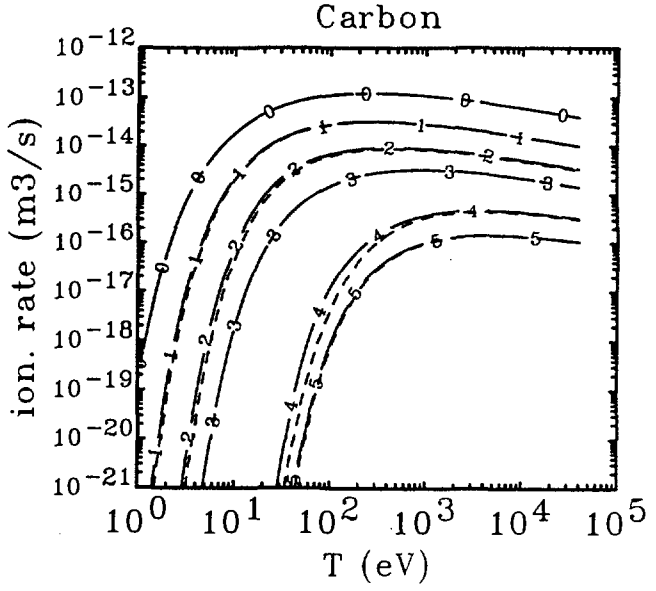

Fig. 9. Rate of ionisation computed for individual charge stages of carbon with (solid line) and without (dashed line) metastable effects.

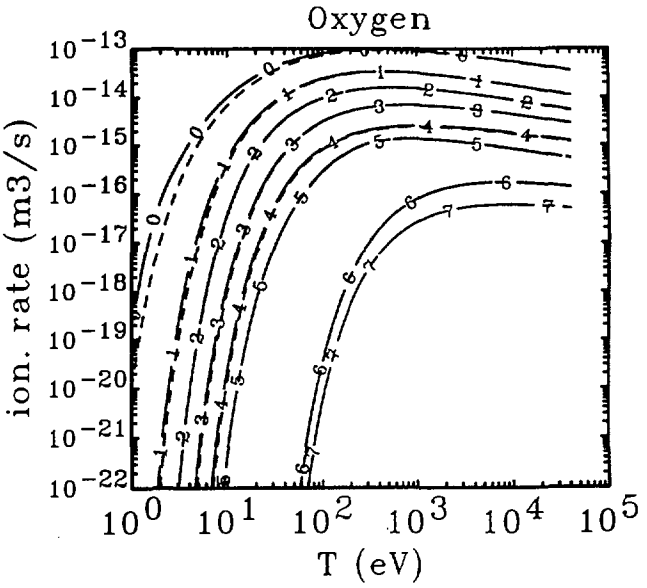

Fig. 10. Rate of ionisation computed for individual charge stages of oxygen with (solid line) and without (dashed line) metastable effects.

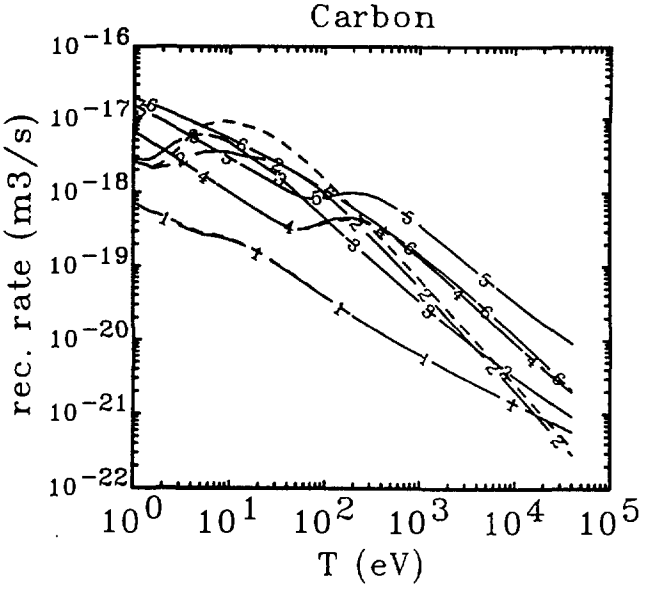

Fig. 11. Rate of radiative plus dielectronic recombination computed for individual charge stages of carbon with (solid line) and without (dashed line) metastable effects.

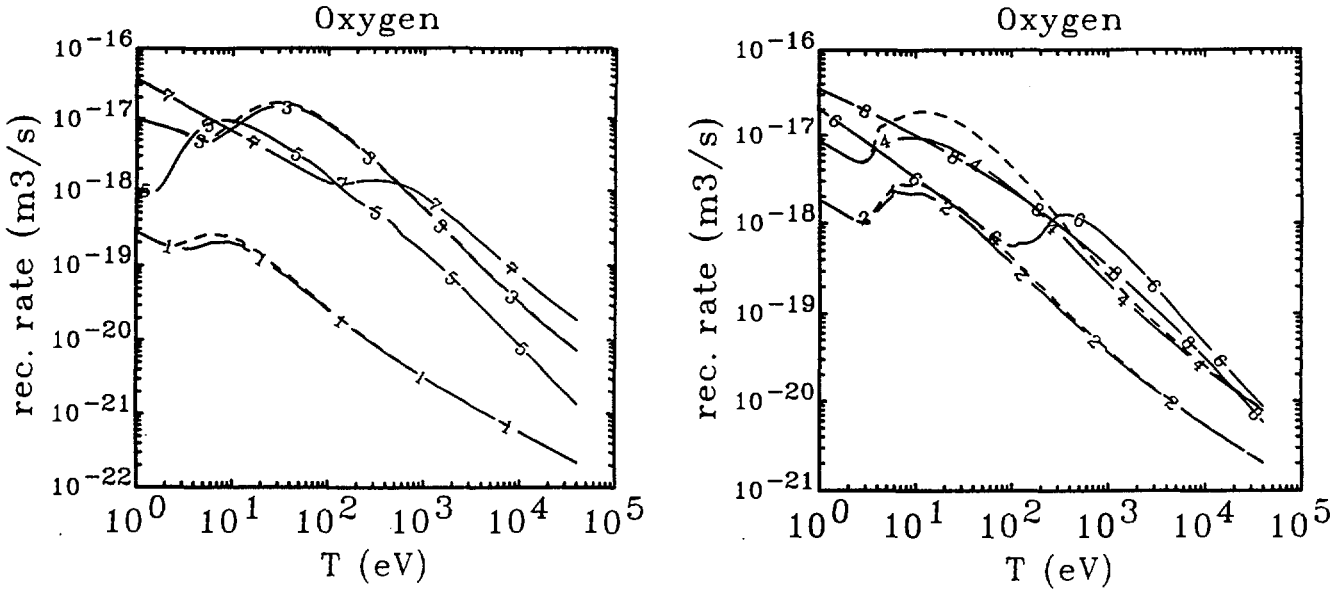

Fig. 12. Rate of radiative plus dielectronic recombination computed for individual charge stages of oxygen with (solid line) and without (dashed line) metastable effects.

4.1.1 Comparisons at steady ionisation balance.

Figures 13 and 14 show the effective charge,

$$Z_{ef} = \sum_i i^2 n_i \Big/ \sum_i i n_i , \qquad (23)$$

calculated for carbon and oxygen at steady ionisation balance with (solid line) and without (dashed line) metastable state effects. As expected, the larger ionisation rates computed with metastable states yield a larger value of the effective charge at a given temperature.

The steady state radiative losses calculated for carbon and oxygen with (solid line) and without (dashed line) metastable effects are shown in Figs. 15 and 16. The largest differences for carbon are found near the local maximum at T≈100eV, where most of the contribution to P_r is from line radiation from helium-like ions. The difference there is of order 30%. For oxygen, the largest difference is found at low temperatures ($T \lesssim 2$eV), where most of contribution to P_r and P_e comes from neutral oxygen.

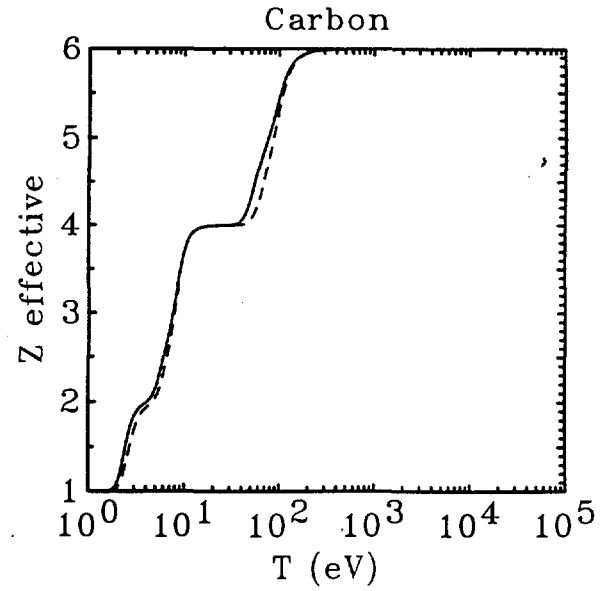

Fig. 13. Effective charge Z_{ef} computed for carbon at steady ionisation balance with (solid line) and without (dashed line) metastable effects.

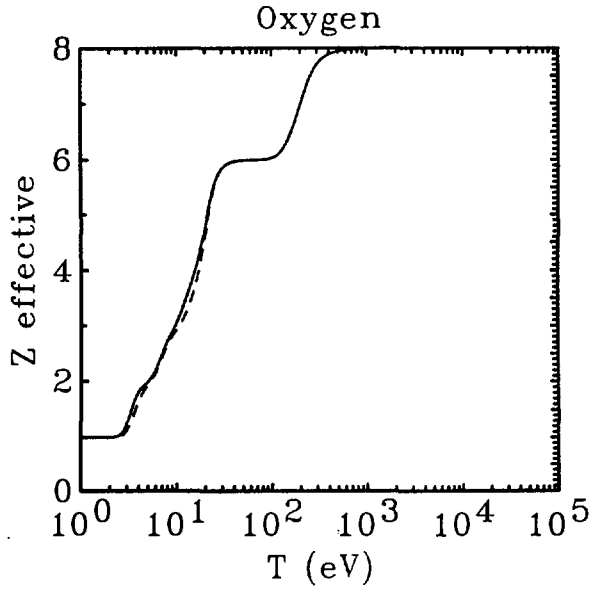

Fig. 14. Effective charge Z_{ef} computed for oxygen at steady ionisation balance with (solid line) and without (dashed line) metastable effects.

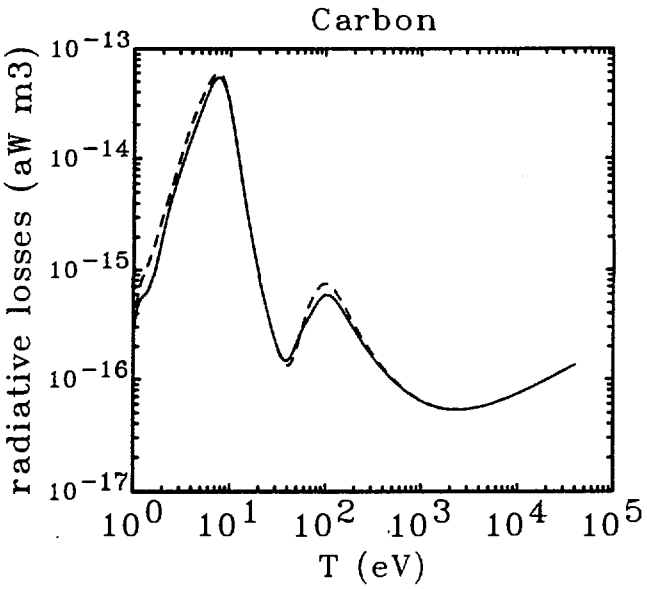

Fig. 15. Radiative power loss function computed for carbon at steady ionisation balance with (solid line) and without (dashed line) metastable effects.

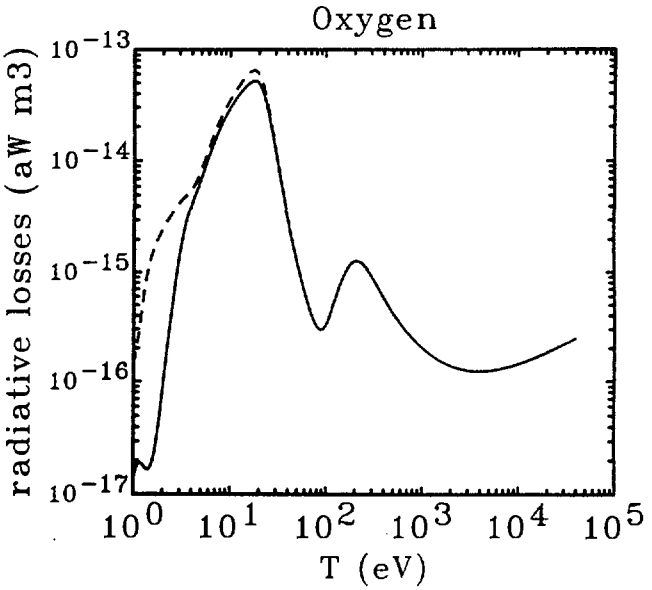

Fig. 16. Radiative power loss function computed for oxygen at steady ionisation balance with (solid line) and without (dashed line) metastable effects.

4.2 Completeness of the recommended excitation rates.

We now assess the completeness of the recommended data base for excitation rates by artificially suppressing semi-empirical excitation rates to the higher excited states, for which no recommended data are available (see Sec. 3.1). First, the usual coronal approximation, which ignores metastable states, is considered. A comparison between the radiative loss coefficients computed for each ionisation stage of carbon and oxygen with (solid line) and without (dashed line) semi-empirical rates is shown in Figs. 17 and 18. A similar comparison is made in Figs. 19 and 20, this time, with the inclusion of metastable effects. The quantitative differences found here are comparable to those found when metastable effects are neglected. For example, the radiative loss computed for OV is reduced by nearly 50% when semi-empirical rates are neglected. The comparison suggests that recommended data are missing, particularly for low ionisation stages at high temperatures. In most cases, the radiative loss coefficients calculated with and without semi-empirical rates are nearly identical at low temperatures. In Fig. 20a the large difference between the two calculations made for neutral oxygen persists down to 1eV. This is because of the relative importance of metastable states at that low temperature (see Fig. 3). Also, the excitation rates for transitions starting from metastable states in OI are mostly semi-empirical.

The effect of semi-empirical rates with metastables is also evident on the steady state radiative loss and cooling functions. Figures 21 and 22 show the radiative loss functions of carbon computed with and without metastable states. In these figures, the rates calculated with and without semi-empirical rates are represented by solid and dashed lines respectively. Figures 23 and 24 give a similar comparison for oxygen. The difference is always larger when metastable states are taken into account. This can be understood by the fact that, in the coronal

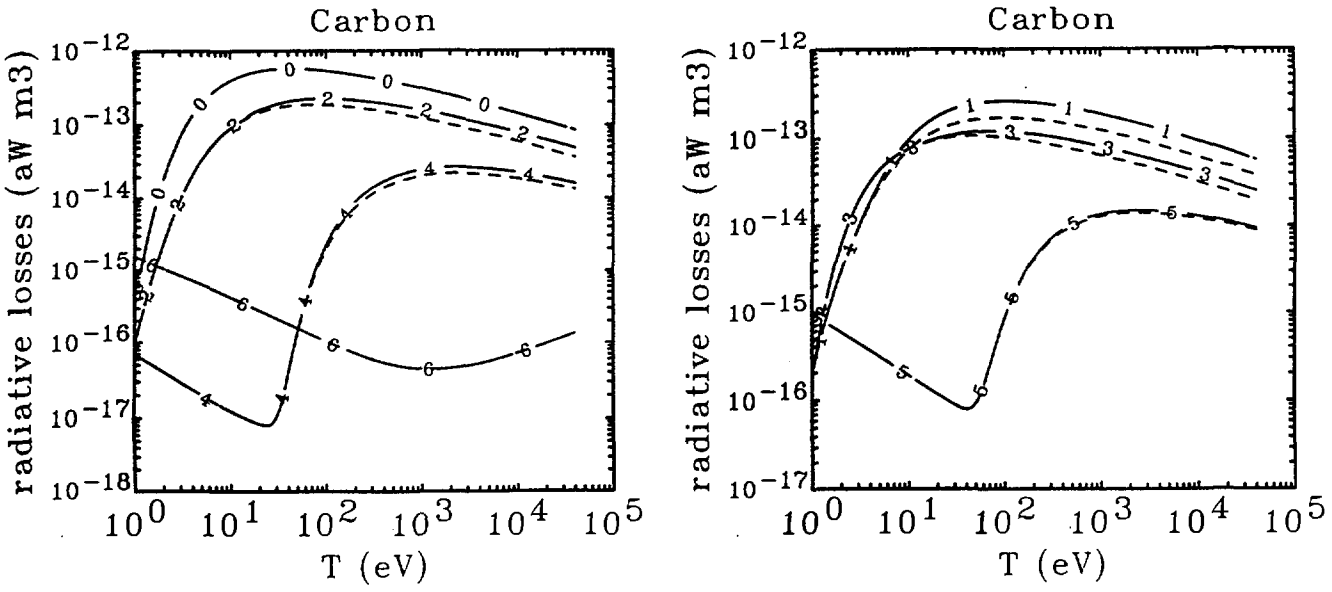

Fig. 17. Radiative loss coefficients for the various ionisation stages of carbon computed, as a function of temperature, with (solid line) and without (dashed line) semi-empirical excitation rates to the higher excited states. In the calculations, metastable states are not taken into account.

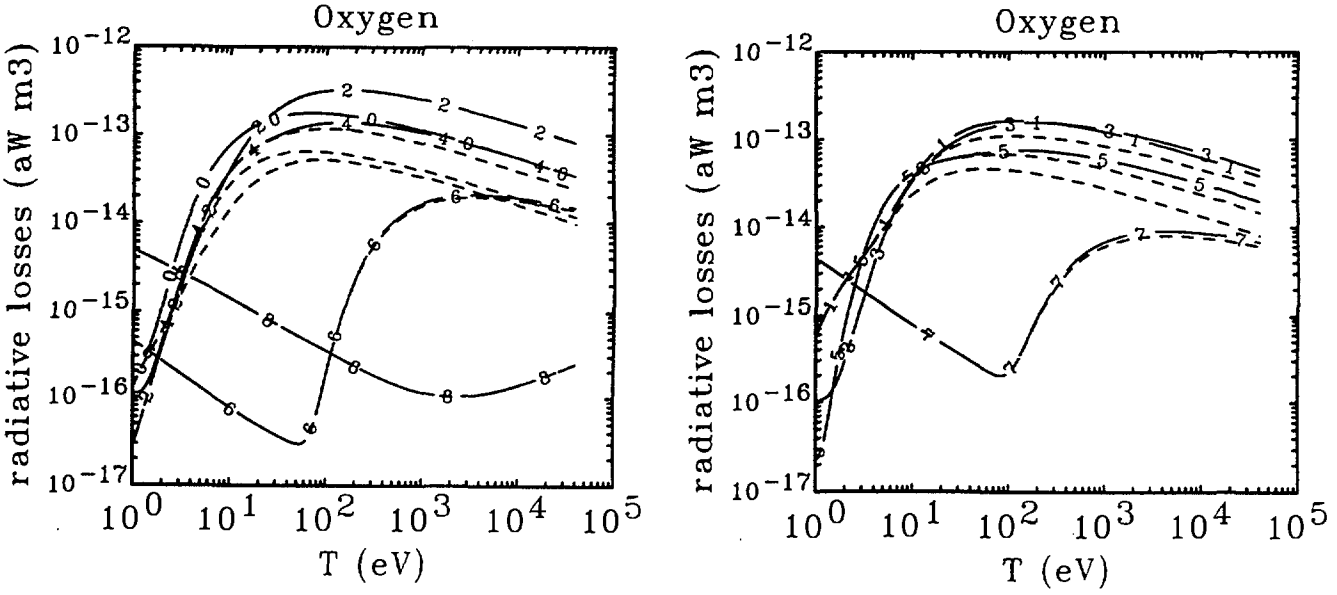

Fig. 18. Radiative loss coefficients for the various ionisation stages of oxygen computed, as a function of temperature, with (solid line) and without (dashed line) semi-empirical excitation rates to the higher excited states. In the calculations, metastable states are not taken into account.

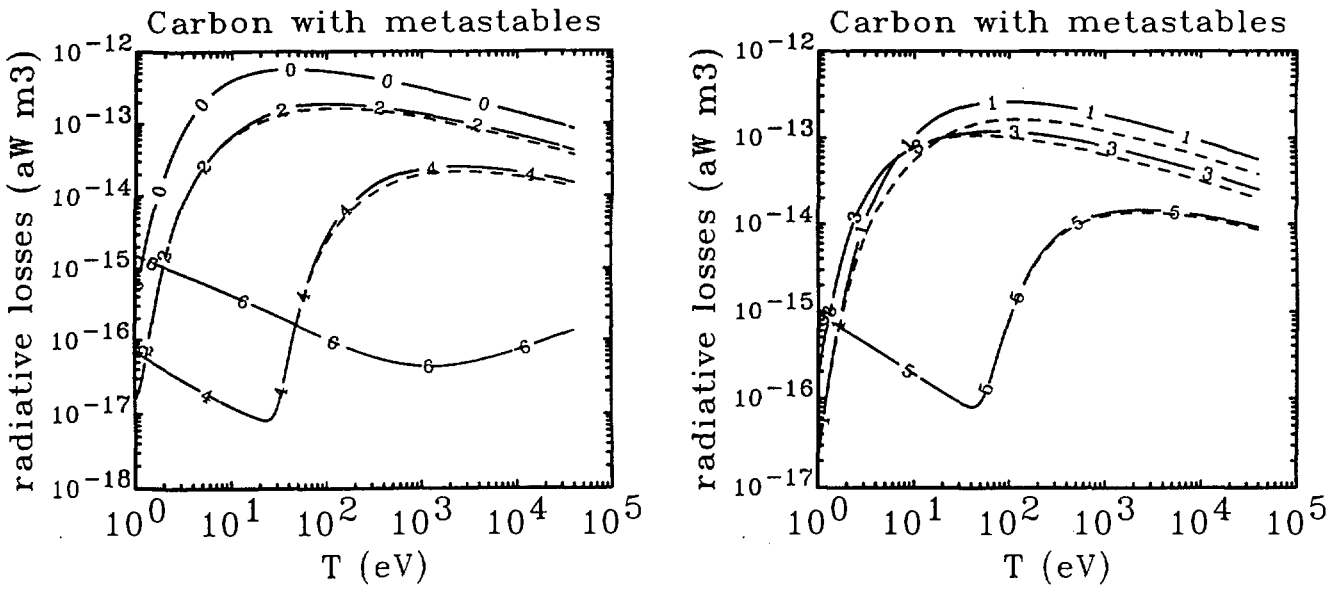

Fig. 19. Radiative loss coefficients for the various ionisation stages of carbon computed, as a function of temperature, with (solid line) and without (dashed line) semi-empirical excitation rates to the higher excited states. In the calculations, metastable states are taken into account.

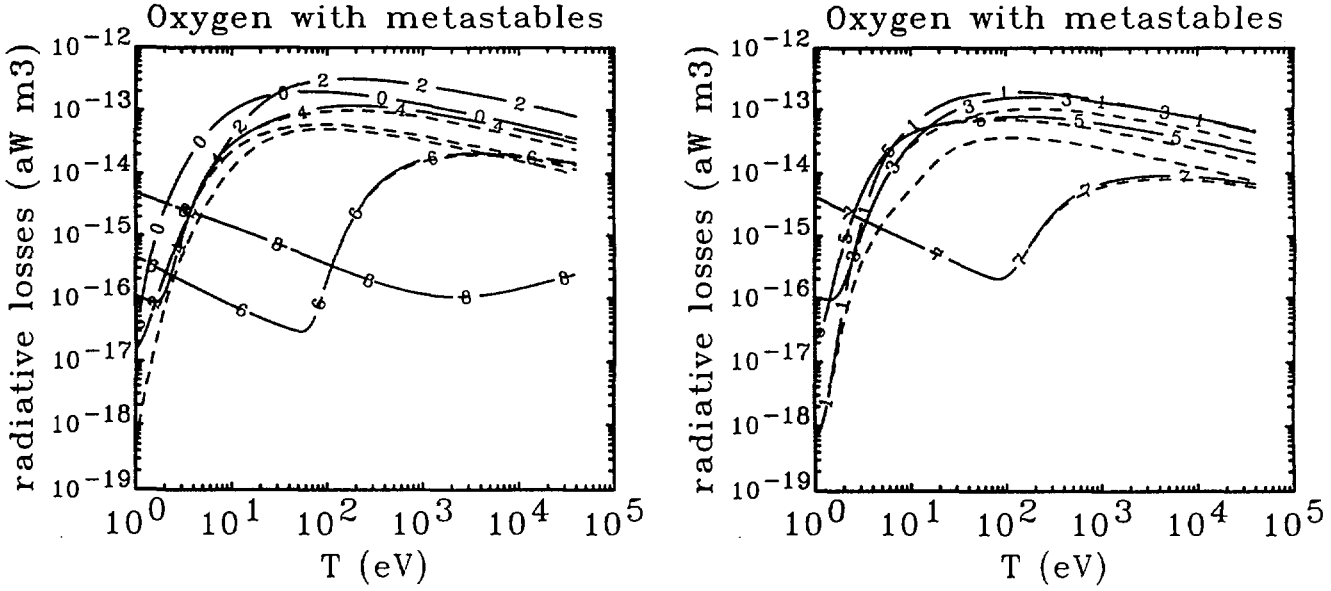

Fig. 20. Radiative loss coefficients for the various ionisation stages of oxygen computed, as a function of temperature, with (solid line) and without (dashed line) semi-empirical excitation rates to the higher excited states. In the calculations, metastable states are taken into account. In Fig. 20a, the lower dashed curve corresponds to neutral oxygen.

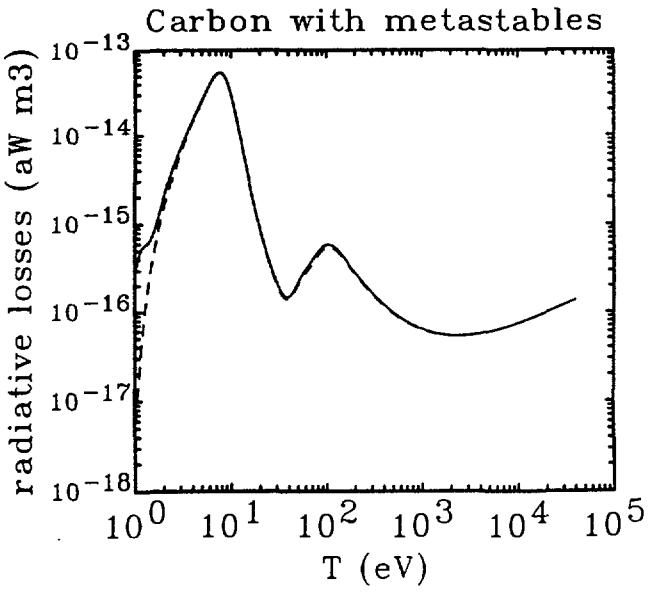

Fig. 21. Radiative loss function computed for carbon at steady ionisation balance with (solid line) and without (dashed line) semi-empirical excitation rates to the higher excited states. In these calculations, the effect of metastable states is taken into account.

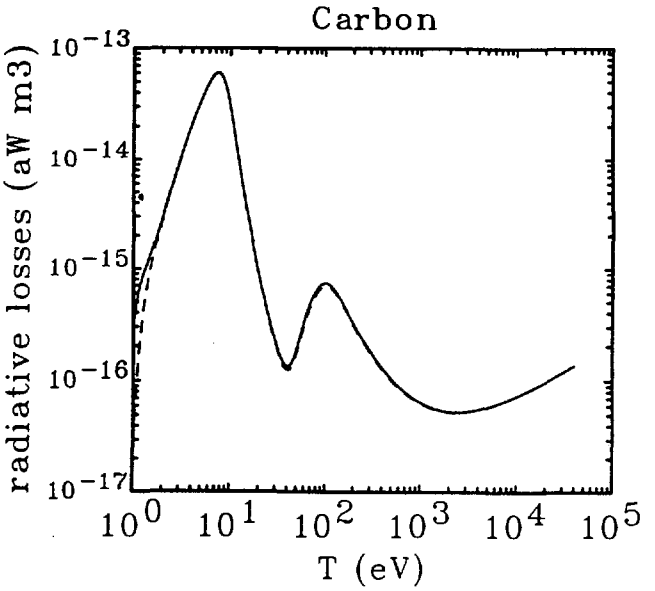

Fig. 22. Radiative loss function computed for carbon at steady ionisation balance with (solid line) and without (dashed line) semi-empirical excitation rates to the higher excited states. In these calculations, the effect of metastable states is not taken into account.

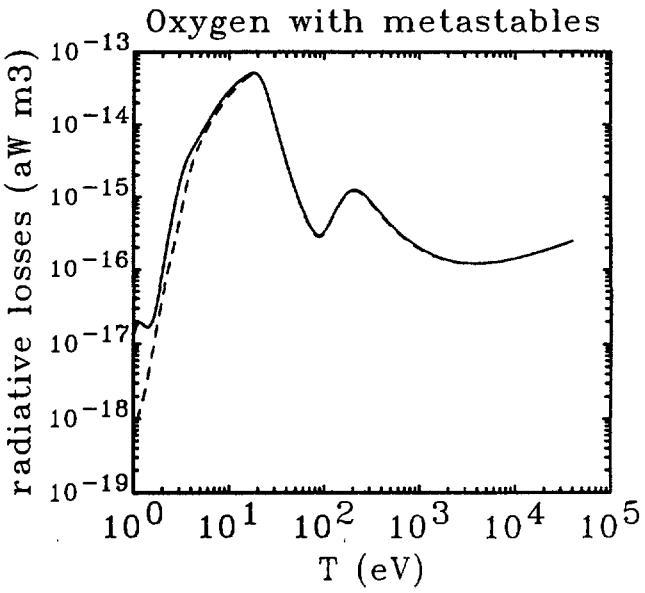

Fig. 23. Radiative loss function computed for oxygen at steady ionisation balance with (solid line) and without (dashed line) semi-empirical excitation rates to the higher excited states. In these calculations, the effect of metastable effects is taken into account.

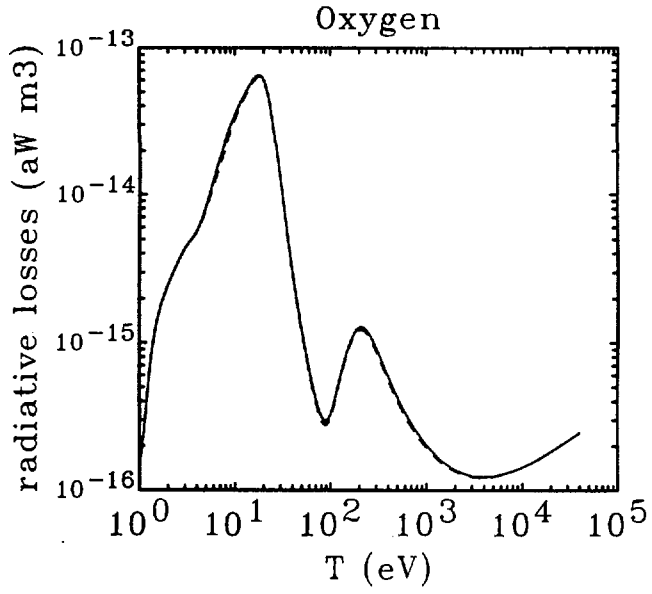

Fig. 24. Radiative loss function computed for oxygen at steady ionisation balance with (solid line) and without (dashed line) semi-empirical excitation rates to the higher excited states. In these calculations, the effect of metastable effects is not taken into account.

approximation, power losses are dominated by $\Delta n=0$ and $\Delta n=1$ transitions. Metastable states often result themselves from $\Delta n=0$ transitions from the ground state. The loss terms computed with metastable states then become less sensitive to $\Delta n=0$ transitions and more sensitive to $\Delta n \geq 1$ transitions, for which data are often missing.

4.3 Comparisons with other approaches.

We now compare our results with those obtained from earlier or simpler calculations. We first consider results obtained by Summers and McWhirter with a model similar to the one described in Sec. 2.3.2. We then consider simpler empirical approaches.

4.3.1 Comparisons with results from Summers and McWhirter.

Detailed calculations of radiative power losses have been made, for example, by Summers and McWhirter (1979). These calculations were done in the usual coronal approximation, which does not account for metastable states, with an assumed electron density of $10^{19} m^{-3}$. The level of atomic physics included in their model is otherwise similar to what is considered here. The loss rates obtained by these authors are qualitatively similar to the ones calculated here and, quantitatively, they generally agree within approximately 50%. A detailed comparison with their radiative loss coefficients is given in Figs. 25 and 26 for all ionisation stages of carbon and oxygen. For the purpose of the comparison, our results are also obtained in the coronal approximation, for an electron density of $10^{19} m^{-3}$. The case of beryllium-like ions is particularly interesting because, in the range of temperatures considered, the loss rates are strongly dominated by excitation followed by radiative decay. Differences in the radiated power therefore directly reflect differences in the excitation rates used in the calculations. These differences are seen to be as large as a factor two for carbon and

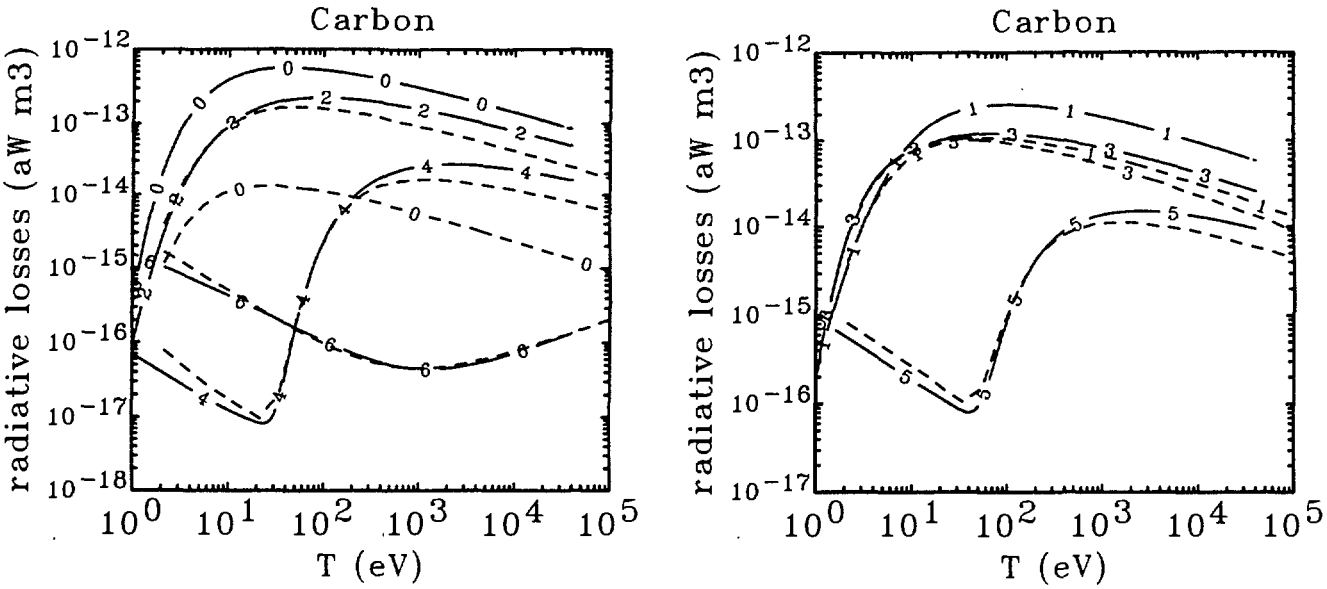

Fig. 25. Radiative loss coefficients calculated for the various ionisation stages of carbon in the coronal approximation. The solid curves give the results of our calculation. The dashed curves show results obtained by Summers and McWhirter.

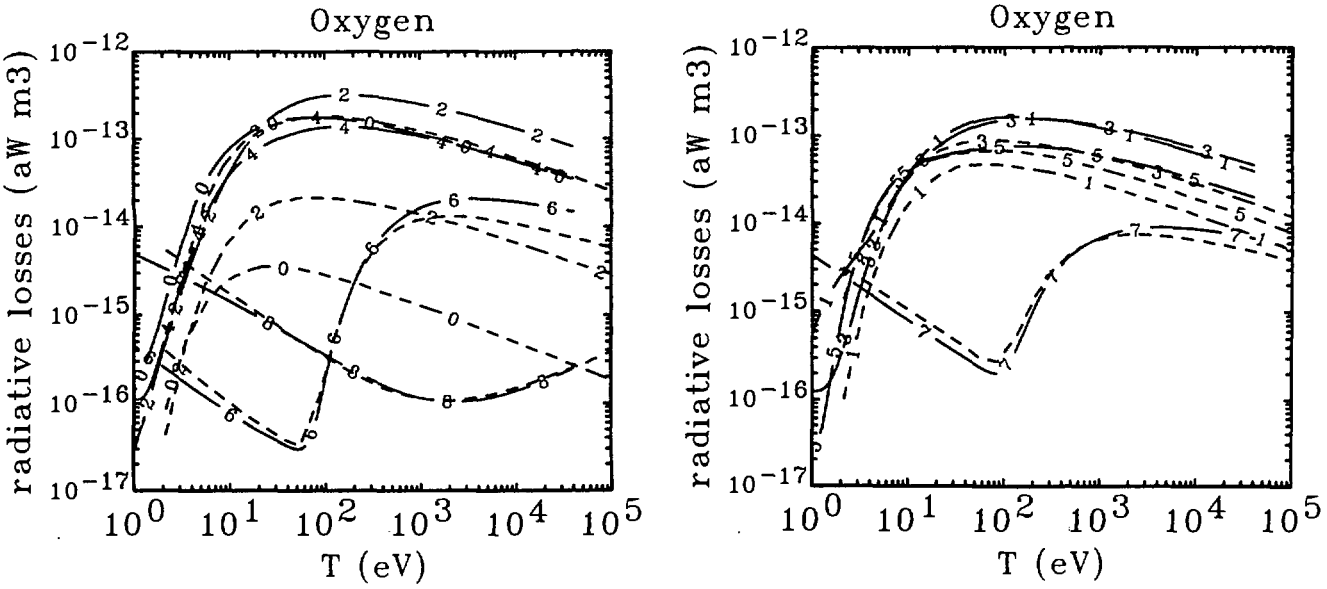

Fig. 26. Radiative loss coefficients calculated for the various ionisation stages of oxygen in the coronal approximation. The solid curves give the results of our calculation. The dashed curves show results obtained by Summers and McWhirter.

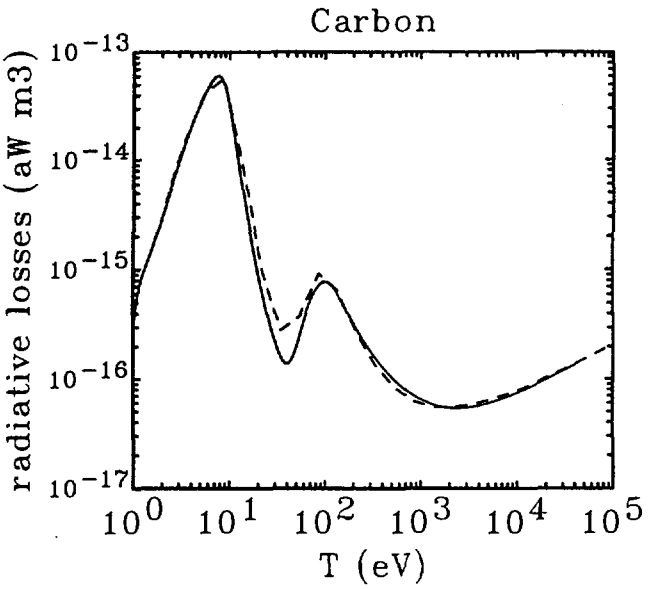

Fig. 27. Radiative loss function calculated for carbon at steady ionisation balance in the coronal approximation. The solid curve gives the result of our calculations. The dashed curve show results obtained by Summers and McWhirter.

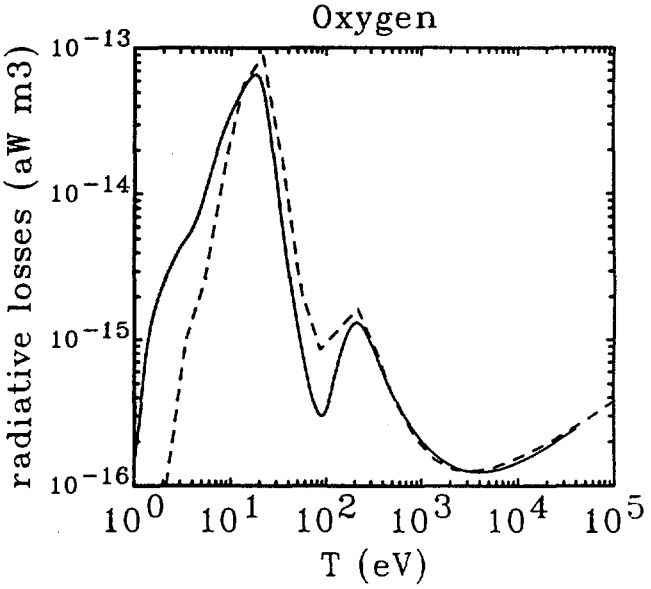

Fig. 28. Radiative loss function calculated for oxygen at steady ionisation balance in the coronal approximation. The solid curve gives the result of our calculations. The dashed curve show results obtained by Summers and McWhirter.

70% for oxygen. Figures 27 and 28 show a comparison between radiative loss functions computed by us (solid line) for carbon and oxygen at steady ionisation balance, and those calculated by Summers and McWhirter (1979). Here again, we find large discrepancies between the two calculations. It is worth noting that differences in the steady state radiative losses may result from a number of different causes. In addition to the rates of excitation, these include differences in the distribution of ionisation stages which, themselves, would result from differences in the ionisation and recombination rates.

4.3.2 Comparisons with simplified approaches.

The effort involved in constructing a comprehensive data base and using it to calculate loss rates is considerable. This can only be justified if it results in significant improvements over simpler approaches. Important quantitative differences are indeed found between our results and those obtained from simplified models. This is illustrated in Figs. 29 to 32, where the average ion charge and the radiative loss functions calculated for carbon and oxygen at steady ionisation balance in the coronal approximation, are compared with results obtained from two relatively simple approaches. The long-dashed curves were obtained with an average ion model (Marchand 1991). The short-dashed curves were obtained from ADPAC (Hulse 1983). This latter calculation accounts for all possible ionisation stages of a given element. It uses recommended ionisation rates for elements up to oxygen. For all other processes, it uses the semi-empirical rates of Post's, et al. (1977) with screened hydrogenic energy levels. The comparison shows important differences between the three approaches. All curves do have the same basic shape. The calculations based on the average ion model, however can be in error by as much as a factor three. The one which uses ADPAC can differ from our results by as much as a factor two.

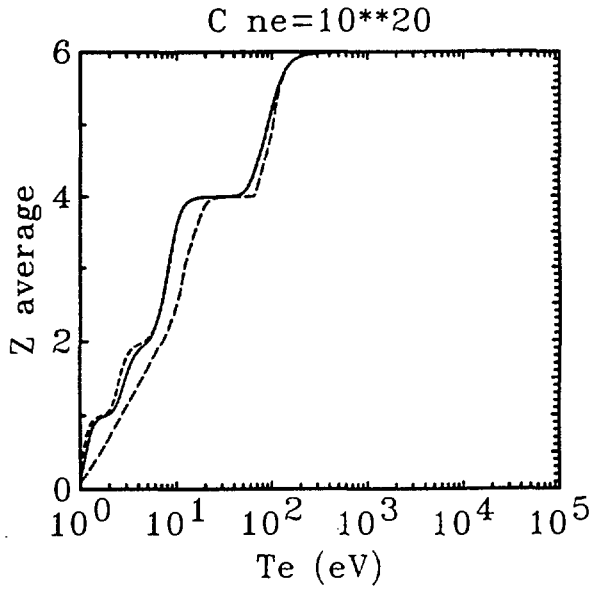

Fig. 29. Average ion charge calculated at steady ionisation balance for carbon in the coronal approximation. In this figure we compare our results (solid line) with those of ADPAC (short dashes) and those of an average ion model (long dashes).

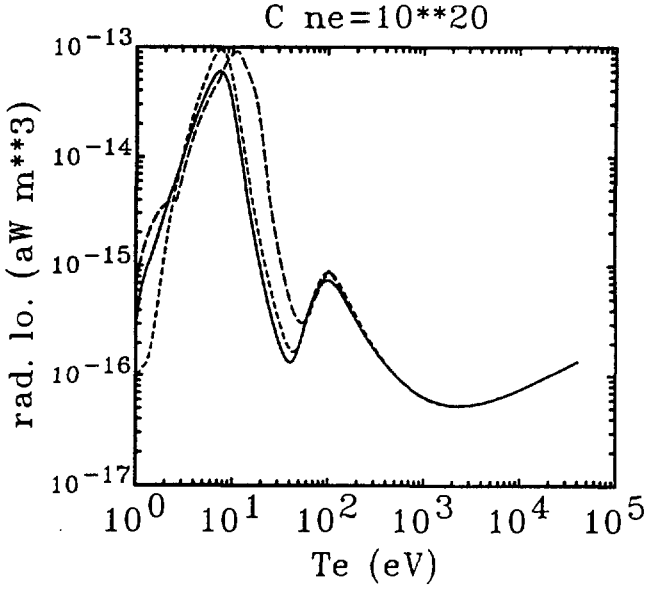

Fig. 30. Steady ionisation balance radiative losses calculated for carbon in the coronal approximation. In this figure we compare our results (solid line) with those of ADPAC (short dashes) and those of an average ion model (long dashes).

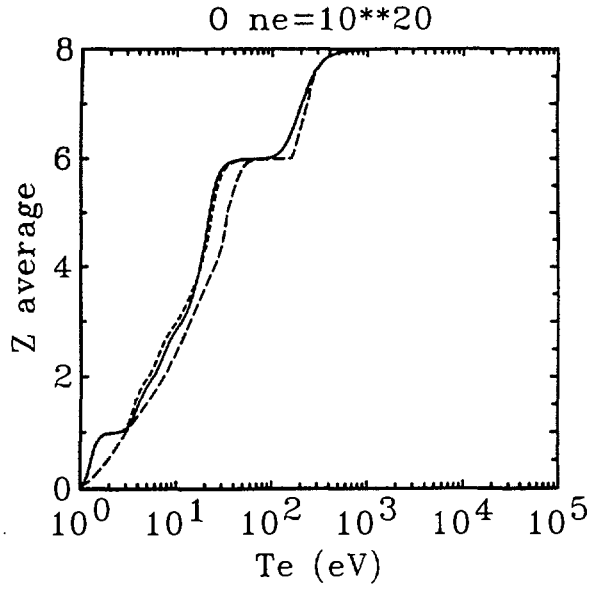

Fig. 31. Average ion charge calculated at steady ionisation balance for oxygen in the coronal approximation. In this figure we compare our results (solid line) with those of ADPAC (short dashes) and those of an average ion model (long dashes).

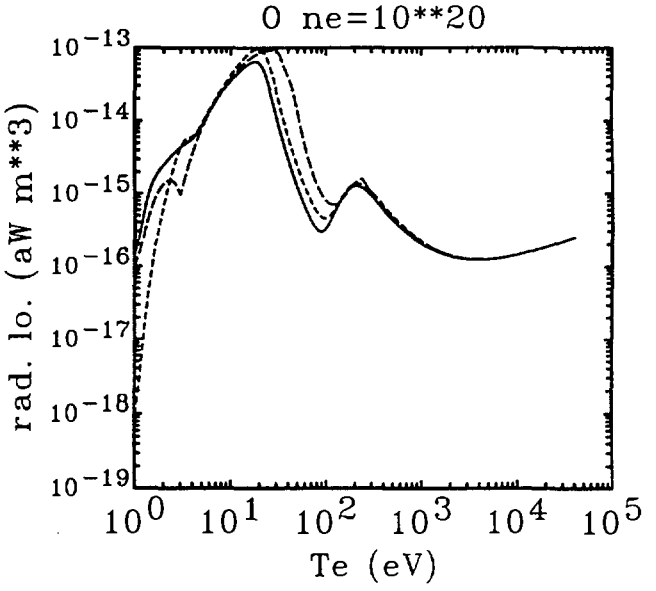

Fig. 32. Steady ionisation balance radiative losses calculated for oxygen in the coronal approximation. In this figure we compare our results (solid line) with those of ADPAC (short dashes) and those of an average ion model (long dashes).

5. Conclusion.

Radiative loss and electron cooling rates have been calculated for carbon and oxygen impurity ions, for plasma conditions of relevance to fusion. The radiative loss function enters the total energy balance. The electron cooling rate enters the electron thermal energy balance. The two rates are equal under steady ionisation balance conditions. They may differ significantly under non steady conditions.

A simple method has been used to calculate loss rates while approximately accounting for the effects of metastable states. The importance of metastable states has been assessed by making comparisons with results obtained in the usual coronal approximation. For both radiative losses and electron cooling rates, significant differences are found.

The completeness of the recommended data basis has been assessed by adding semi-empirical rates to higher excitation states than those for which recommended data are available. For individual ionisation stages, the effect of including semi-empirical rates can be significant, particularly for low ionisation stages at high temperatures. For radiative loss functions at steady ionisation balance, the inclusion of semi-empirical rates is found to more important when metastable states are included in the calculation.

Comparisons with earlier calculations of radiative losses reveal important quantitative differences. This shows the necessity of using recommended and accurate data in the calculation of atomic related power losses.

In summary, we have produced comprehensive calculations of radiative losses and electron cooling rates for carbon and oxygen in plasmas. Our model accounts for the effect of metastable states, and it is based on the most recent recommended atomic data. We stress that such

calculations are contingent upon the availability and accuracy of data for a wealth of atomic processes. We would like to end this report with a short list of processes for which more accurate or detailed data are required. These are:

a) Excitation.

When metastable states are taken into account, excitation to higher states become significant. In practice, those would correspond to transitions with Δn up to two, from the ground state.

b) Ionisation.

Recommended data for the ionisation cross sections typically account for a number of processes. For example,

$$e + OV(1s^2 2s^2) \rightarrow e + e + OVI(1s^2 2s)$$

$$e + OV(1s^2 2s^2) \rightarrow e + e + OVI(1s2s^2) \begin{cases} \rightarrow e + e + e + OVII(1s^2) \\ \rightarrow e + e + h\nu + OVI(1s^2 2s) \end{cases}$$

$$e + OV(1s^2 2s^2) \rightarrow e + OV(1s2s^2 2p) \begin{cases} \rightarrow e + e + OVI(1s^2 2s) \\ \rightarrow e + h\nu + OV(1s^2 2s^2) \\ \vdots \quad \ldots \end{cases}$$

Because these processes have different energy thresholds, they will contribute differently to the radiative losses and electron cooling rates. Accurate cross sections and, when appropriate, Auger rates and branching ratios are therefore required for each process.

c) Dielectronic recombination.

Cross sections for dielectronic recombination corresponding to specific transitions are required. The results presented here have relied largely on scaled hydrogenic rates that were normalized to reproduce recommended total recombination rates. Accurate calculations with finite density effects are needed.

d) Radiative recombination.

Detailed cross sections for radiative recombination to specific states are needed. This includes recombination into metastable states, from ions initially in the ground or metastable states.

e) Transition probabilities.

Several transition probabilities needed to calculate the relative populations of the ground and metastable states are missing and had to be evaluated from scaled hydrogenic values.

References.

- S.M.V. Aldrovandi and D. Péquignot, Astron. Astrophys. 25, 137 (1973).
- N.R. Badnell, J. Phys. B 20, 2081 (1987).
- N.R. Badnell, J. Phys. B 21, 749 (1988).
- N.R. Badnell, Phys. Scripta T28, 33 (1989).
- D.R. Bates, A.E. Kingston, and R.W.P. McWhirter, Proc. R. Soc. A 267, 297 (1962).
- B.J. Braams, "A Multifluid Code for Simulation of the Edge Plasma in Tokamaks", NET Report EUR-FU/XII-80/87/68 (1987).
- S. Chandrasekar, "An Introduction to the study of Stellar Structure", (University of Chicago Press, Chicago, 1939), Chap. VII.
- S. Datz and P.F. Dittner, Z. Phys. D 10, 187 (1988).
- G.W.F. Drake, Phys. Rev. A 3, 908 (1971).
- G.W.F. Drake, Phys. Rev. A 34, 2871 (1986).
- P.L. Dufton, K.A. Berrington, P.G. Burke, and A.E. Kingston, Astron. Astrophys. 62, 111 (1978).
- D.C. Griffin, Phys. Scripta T28, 17 (1989).
- Y. Hahn, Phys. Scripta T28, 25 (1989).
- R. Hulse, Nucl. Technol./Fusion 3, 259 (1983).
- Y.Itikawa, S. Hara, T. Kato, S. Nakazaki, M.S. Pindzola, and D.H. Crandall, Atom. Data Nucl. Data Tables 33, 149 (1985).

- Y. Itikawa, K. Sakimoto, and S. Nakazaki, Phys. Rev. A 36, 1088 (1987).
- Y. Itikawa and A. Ichimura, J. Phys. Chem. Ref. Data 19, 637 (1990).
- T. Kato and S. Nakazaki, Atom. Data Nucl. Data Tables 42, 313 (1989).
- T. Kato, J. Lang, and K.E. Berrington, Atom. Data Nucl. Data Tables 44, 133 (1990).
- R.R. Laher and F.R. Gilmore, J. Phys. Chem. Ref. Data 19, 277 (1990).
- M.A. Lennon, K.L. Bell, H.B. Gilbody, J.G. Hughes, E. Kingston, M.J. Murray, and F.J. Smith, J. Phys. Chem. Ref. Data 17, 1285 (1988).
- W.A. Lokke and W.H. Grasberger, "XSNQ-U: A Non-LTE Emission and Absorption Coefficient Subroutine", UCRL-52276 (1977).
- R. Marchand, S. Caillé, and Y.T. Lee, J. Quant. Spectrosc. Radiat. Transfer 43, 149 (1990).
- R. Marchand, private communication. Based in part on work done under NET contract NET/90-815 (1991).
- R.M. More, J. Quant Spectrosc. Radiat. Transfer 27, 345 (1982).
- R.W.P. McWhirter and H.P. Summers, Applied Atom. Coll. Phys. 2, 51 (1984).
- R.A. Phaneuf, R.K. Janev, and M.S. Pindzola "Collisions of Carbon and Oxygen Ions with Electrons, H, H_2 and He", Atomic Data for Fusion, Volume 5, ORNL-6090 (1987).
- D.E. Post, R.V. Jensen, C.B. Tarter, W.H. Gasberger, and W.A. Lokke, Atom. Data and Nucl. Data Tables 20, 397 (1977).
- L.J. Roszman, Phys. Scripta T28, 36 (1989).
- V.P. Shevelko, L.A. Vainshtein, and E.A. Yukov, Phys. Scripta T28, 39 (1989).
- B Strômgren, Z. Astrophys. 4, 118 (1932).
- H.P. Summers and M.B. Hooper, Plasma Phys. 25, 1331 (1983).
- H.P. Summers and R.W.P. McWhirter, J. Phys. B 12, 2387 (1979).
- H.P. Summers, Mont. Not. R. Astron. Soc. 178, 101 (1977).

- W.L. Wiese and J.R. Fuhr, private communication (1991).
- W.L. Wiese, M.W. Smith, and B.M. Glennon, "Atomic Transition Probabilities, Volume I Hydrogen through Neon", Natl. Standard Ref. Data Ser. Nat. Bur. Stand. (U.S.) 4, U.S. Government Print. Office, Washington, D.C. (1966).

Appendix A. List of states considered in the calculations.

In this appendix, we list the states considered in the calculation of P_r and P_e for individual carbon and oxygen ions. The ground, metastable and autoionizing states are identified at the right of the corresponding rows. For each state we also give the energy and degeneracy. The energy is defined such that an ion in its ground state has an energy equal to minus its ionisation energy.

CI

State index	Energy (eV)	Degeneracy	Configuration	
1	-11.264	9	$1s^2 2s^2 2p^2\ ^3P$	ground

CII

State index	Energy (eV)	Degeneracy	Configuration	
1	-24.376	6	$1s^2 2s^2 2p\ ^2P$	ground
2	-19.046	12	$2s2p^2\ ^4P$	metastable
3	-15.086	10	^2D	
4	-12.416	2	^2S	
5	-10.666	6	^2P	
6	- 9.926	2	$2s^2 3s\ ^2S$	
7	- 8.046	6	$3p\ ^2P$	
8	- 6.326	10	$3d\ ^2D$	

CIII

State index	Energy (eV)	Degeneracy	Configuration		
1	-47.864	1	$1s^2 2s^2$	^1S	ground
2	-41.364	9	$2s2p$	^3P	metastable
3	-35.174	3		^1P	
4	-30.824	9	$2p^2$	^3P	
5	-29.774	5		^1D	
6	-25.234	1		^1S	
7	-18.334	3	$2s3s$	^3S	
8	-17.224	1		^1S	
9	-15.764	3	$3p$	^1P	
10	-15.664	9		^3P	
11	-14.384	15	$3d$	^3D	
12	-13.584	5		^1D	

CIV

State index	Energy (eV)	Degeneracy	Configuration		
1	-64.476	2	$1s^2 2s$	^2S	ground
2	-56.476	6	2p	^2P	
3	-26.926	2	3s	^2S	
4	-24.796	6	3p	^2P	
5	-24.196	10	3d	^2D	
6	229.135	2	$1s2s^2$	^2S	autoionizing
7	232.400	12	2s2p	^4P	
8	237.298	6	$2s(^1S)2p$	^2P	
9	242.332	6	$2s(^3S)2p$	^2P	

CV

State index	Energy (eV)	Degeneracy	Configuration		
1	-391.986	1	$1s^2$	^1S	ground
2	- 93.036	3	1s2s	^3S	metastable
3	- 87.586	1		^1S	metastable
4	- 87.586	9	1s2p	^3P	
5	- 84.086	3		^1P	
6	- 45.833	3	1s3s	^3S	
7	- 44.850	1		^1S	
8	- 38.466	9	1s3p	^3P	
9	- 37.686	15	1s3d	^3D	
10	- 37.679	3		^1D	
11	- 37.486	3	1s3p	^1P	

CVI

State index	Energy (eV)	Degeneracy	Configuration	
1	-489.84	2	1s	ground
2	-122.34	2	2s	metastable
3	-122.34	6	2p	
4	- 54.44	2	3s	
5	- 54.34	6	3p	
6	- 54.24	10	3d	
7	- 30.44	2	4s	
8	- 30.44	6	4p	
9	- 30.44	10	4d	
10	- 30.44	14	4f	
11	- 19.44	6	5p	

OI

State index	Energy (eV)	Degeneracy	Configuration		
1	-13.618	9	$1s^2 2s^2 2p^4$	^3P	ground
2	-11.651	5		^1D	metastable
3	- 9.428	1		^1S	metastable
4	- 4.472	5	$2p^3(^4S)3s$	^5S	metastable
5	- 4.097	3		^3S	
6	- 2.878	15	3p	^5P	
7	- 2.628	9		^3P	
8	- 1.778	5	4s	^5S	
9	- 1.688	3		^3S	
10	- 1.538	25	3d	^5D	
11	- 1.528	15		^3D	
12	- 1.328	15	4p	^5P	
13	- 1.258	9		^3P	
14	- 1.078	15	$(^2D)3s$	^3D	
15	- 0.888	5		^1D	
16	- 0.868	25	$(^4S)4d$	^5D	
17	- 0.858	15		^1D	
18	0.502	9	$(^2P)3s$	^3P	autoionizing
19	0.742	3		^1P	
20	1.552	15	$(^2D)4d$	^3D	
21	1.602	5		^1D	
22	1.672	9	3d	^3P	
23	1.742	3		^3S	
24	1.742	15		^3D	
25	2.042	9	$2s2p^5$	^3P	
26	2.492	9	$2s^2 2p^3(^2D)4d$	^3P	
27	3.282	3	$(^2P)4s$	^1P	
28	3.472	9	3d	^3P	
29	3.472	15		^3D	
30	3.472	21		^3F	
31	4.152	21	4d	^3F	

OII

State index	Energy (eV)	Degeneracy	Configuration		
1	-35.108	4	$1s^2 2s^2 2p^3$	^4S	ground
2	-31.784	10		^2D	metastable
3	-30.092	6		^2P	metastable
4	-20.242	12	$2s2p^4$	^4P	
5	-12.127	12	$2s^2 2p^2 3s$	^4P	

OIII

State index	Energy (eV)	Degeneracy	Configuration		
1	-54.886	9	$1s^2 2s^2 2p^2$	^3P	ground
2	-52.396	5		^1D	metastable
3	-49.556	1		^1S	metastable
4	-47.436	5	$2s2p^3$	^5S	metastable
5	-40.026	15		^3D	
6	-37.256	9		^3P	
7	-31.726	5		^1D	
8	-30.486	3		^3S	
9	-28.826	3		^1P	

OIV

State index	Energy (eV)	Degeneracy	Configuration		
1	-77.394	6	$1s^2 2s^2 2p$	^2P	ground
2	-68.577	12	$2s2p^2$	^4P	metastable
3	-61.684	10		^2D	
4	-57.044	2		^2S	
5	-55.034	6		^2P	
6	-33.054	2	$2s^2 3s$	^2S	
7	-25.374	10	3d	^2D	

OV

State index	Energy (eV)	Degeneracy	Configuration		
1	-113.873	1	$1s^2 2s^2$	^1S	ground
2	-103.673	9	2s2p	^3P	metastable
3	- 94.193	3		^1P	
4	- 87.373	9	$2p^2$	^3P	
5	- 85.373	5		^1D	
6	- 78.183	1		^1S	
7	- 46.053	3	2s3s	^3S	
8	- 44.303	1		^1S	
9	- 41.883	3	3p	^1P	
10	- 41.603	9		^3P	
11	- 39.383	15	3d	^3D	
12	- 37.943	5		^1D	

OVI

State index	Energy (eV)	Degeneracy	Configuration		
1	-138.080	2	$1s^2 2s$	^2S	ground
2	-126.100	6	2p	^2P	
3	- 58.730	2	3s	^2S	
4	- 55.480	6	3p	^2P	
5	- 54.440	10	3d	^2D	
6	414.311	2	$1s2s^2$	^2S	autoionizing
7	418.393	12	2s2p	^4P	
8	426.556	6	$2s(^1S)2p$	^2P	
9	432.816	6	$2s(^3S)2p$	^2P	

OVII

State index	Energy (eV)	Degeneracy	Configuration		
1	-739.114	1	$1s^2$	^1S	ground
2	-178.114	3	1s2s	^3S	metastable
3	-170.514	9	2p	^3P	
4	-170.414	1	2s	^1S	metastable
5	-165.214	3	2p	^1P	
6	- 77.214	3	3s	^3S	
7	- 75.114	9	3p	^3P	
8	- 75.014	1	3s	^1S	
9	- 74.014	15	3d	^3D	
10	- 73.914	5	3d	^1D	
11	- 73.514	3	3p	^1P	
12	- 45.484	9	4p	^3P	
13	- 44.804	5	4d	^1D	
14	- 43.460	1	4s	^1S	
15	- 42.763	3	4p	^1P	
16	- 42.756	15	4d	^3D	
17	- 30.109	5	5d	^1D	
18	- 28.222	1	5s	^1S	
19	- 27.873	3	5p	^1P	
20	- 27.654	9		^3P	
21	- 27.654	15	5d	^3D	
22	- 19.949	1	6s	^1S	
23	- 19.775	3	6p	^3P	

OVIII

State index	Energy (eV)	Degeneracy	Configuration	
1	-870.272	2	1s	ground
2	-216.772	2	2s	metastable
3	-216.672	6	2p	
4	- 96.672	2	3s	
5	- 96.672	6	3p	
6	- 96.672	10	3d	
7	- 54.384	2	4s	
8	- 54.384	6	4p	
9	- 54.384	10	4d	
10	- 54.384	14	4f	

Appendix B. Scaling of dielectronic recombination for carbon and oxygen ions.

The level of scaling refers to cases a, b, c, d or e as explained in Sec. 3.4. For clarity, level a is identified here as ∀, level b by $\Delta n=0$ or $\Delta n=1$, level c by $\Delta n>0$, level d by the index of the final state, and level e by autoionizing.

CII

initial state index	level	reference
1	∀	Badnell (1989)
2	∀	"
1	$\Delta n=0$	Hahn (1989)
1	3	Badnell (1988)
1	5	"

CIII

initial state index	level	reference
1	∀	Datz and Dittner (1988)
1	$\Delta n=0$	Griffin (1989)
2	∀	Badnell (1989)
1	3	Badnell (1987)

CIV

initial state index	level	reference
1	∀	Badnell (1989)

CV

initial state index	level	reference
1	∀	Griffin (1989)

CVI

initial state index	level	reference
1	∀	Hahn (1989)

OII

initial state index	level	reference
1	∀	Badnell (1989)
2	∀	"
3	∀	"

OIII

initial state index	level	reference
1	∀	Roszman (1989)
2	∀	Badnell (1989)
3	∀	"
4	∀	"

OIV

initial state index	level	reference
1	∀	Badnell (1989)
1	Δn=0	Hahn (1989)
2	∀	Badnell (1989)
1	3	Badnell (1988)
1	4	"
1	5	"
1	6	"
1	7	"

OV

initial state index	level	reference
1	∀	Badnell (1989)
1	Δn=0	Griffin (1989)
1	Δn=1	"
2	∀	Badnell (1989)
1	3	Badnell (1987)

OVI

initial state index	level	reference
1	Δn=0	Griffin (1989)
1	Δn>0	"
1	autoionizing	"

OVII

initial state index	level	reference
1	∀	Griffin (1989)

OVIII

initial state index	level	reference
1	∀	Hahn (1989)

Appendix C. Radiative and electron cooling rates for individual ionisation stages of carbon and oxygen.

This appendix gives the main results of our calculations; that is the radiative and cooling rate coefficients calculated with the model presented in Sec. 2.3.4, and the data described in Sec. 3. The rates are given in units of attowatts m^3. We recall that 1 aW = 10^{-18}W. For radiative losses, we distinguish between the following contributions:

a - line radiation associated with excitation by direct collisional impact and dielectronic recombination (long dashes),

b - bremsstrahlung (alternating long and short dashes),

c - continuum radiation associated with radiative recombination (medium dashes), and

d - radiative cascade following radiative and dielectronic recombinations (short dashes).

Note that in part d, only the cascade of the electron captured in a group of Rydberg states is considered. The contribution from excitation of a core electron is already included in part a.

In the calculation of electron cooling rates, the following contributions are considered:

a - excitation by direct collisional impact or associated with dielectronic recombination, minus collisional deexcitation from metastable states, (long dashes),

b - bremsstrahlung (alternating long and short dashes),

c - the loss of electron kinetic energy (see contribution 1, Fig. 1) associated with radiative and dielectronic recombinations (medium dashes), and

d - ionisation (short dashes).

The total power loss coefficients are shown as solid curves.

For ionisation stages below helium-like, radiative loss rates are dominated by line radiation. Electron cooling rates are dominated by excitation and, at the higher temperatures, also by ionisation. As a result, P_r and P_e generally have comparable numerical values, except at higher temperatures, where $P_e > P_r$. This observation is consistent with the remark made in Sec. 2.2 that P_e should be larger than P_r when the ions are ionizing.

Helium and hydrogen like ions are characterized by two distinct regimes. At low temperatures, P_r is dominated by radiative cascade and continuum radiation, while P_e is dominated by the rate at which recombining electrons loose their kinetic energy. P_r is then always larger than P_e and the difference between P_r and P_e increases as the temperature decreases. At higher temperatures, the various contributions are approximately in the same proportions as for the lower ionisation stages. The largest differences between P_r and P_e are found for fully ionized ions when recombination is dominant (when $T \lesssim 1$keV). As pointed out in Sec. 2.3.4, the approximate model used here to account for metastable states is only valid provided recombination does not contribute significantly to the loss rates. This condition breaks down for the higher ionisation stages, at low temperatures. In this case, our model effectively reduces to the usual coronal model which ignores the effect of metastable states. Detailed results are given in the figures which follow.

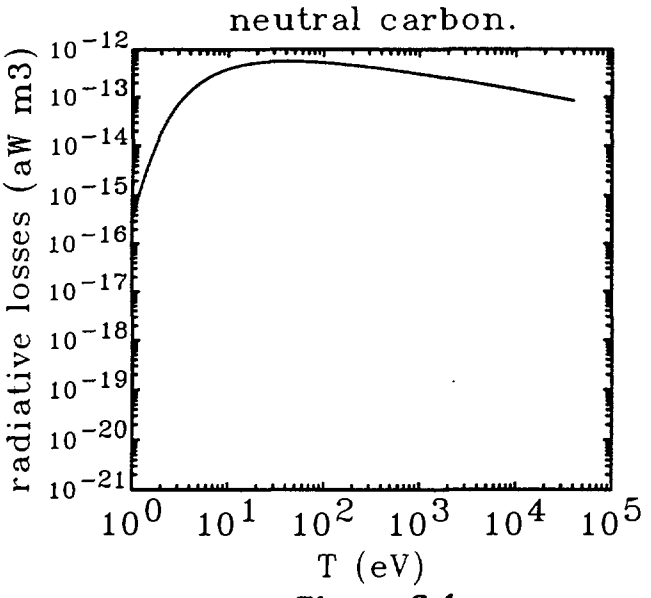

Figure C-1

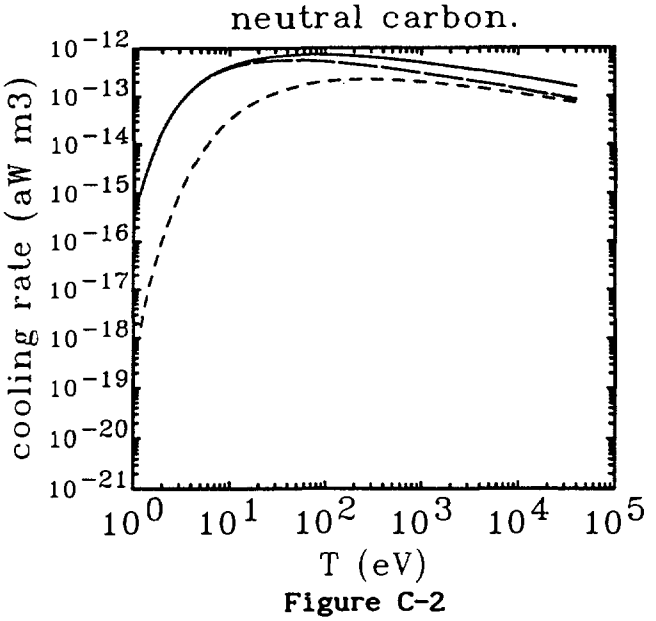

Figure C-2

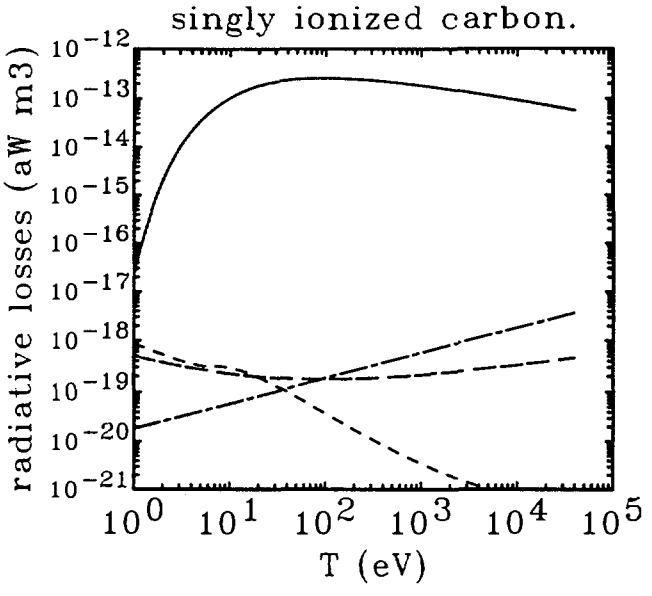

Figure C-3

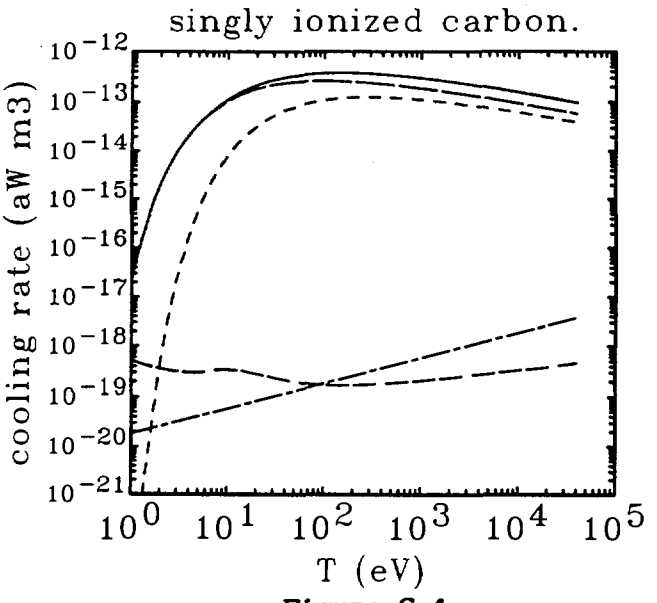

Figure C-4

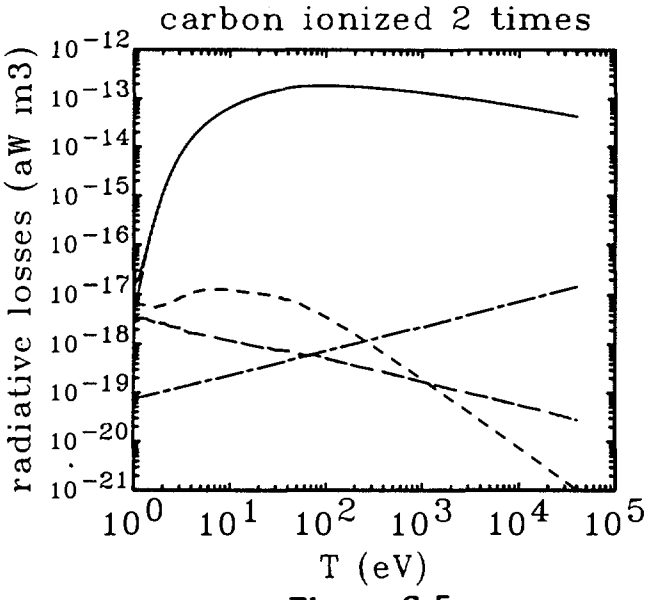

Figure C-5

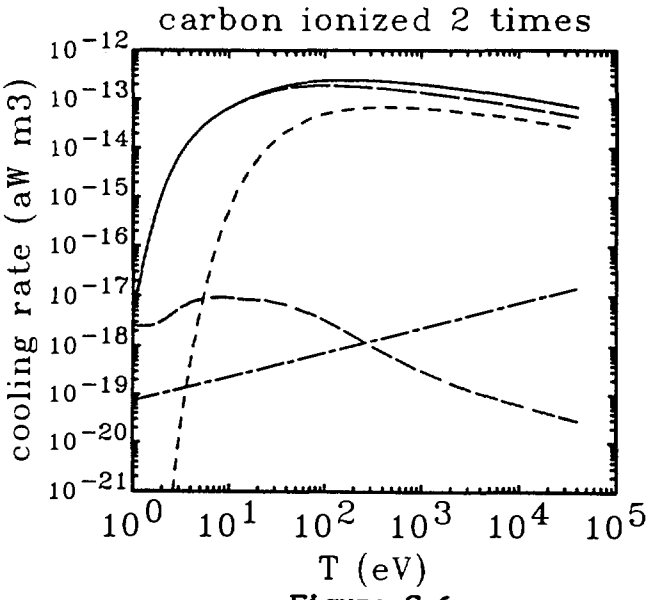

Figure C-6

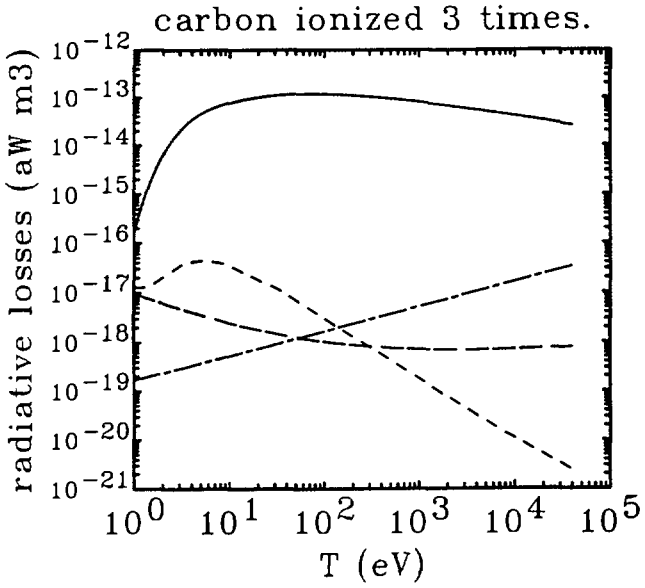

Figure C-7

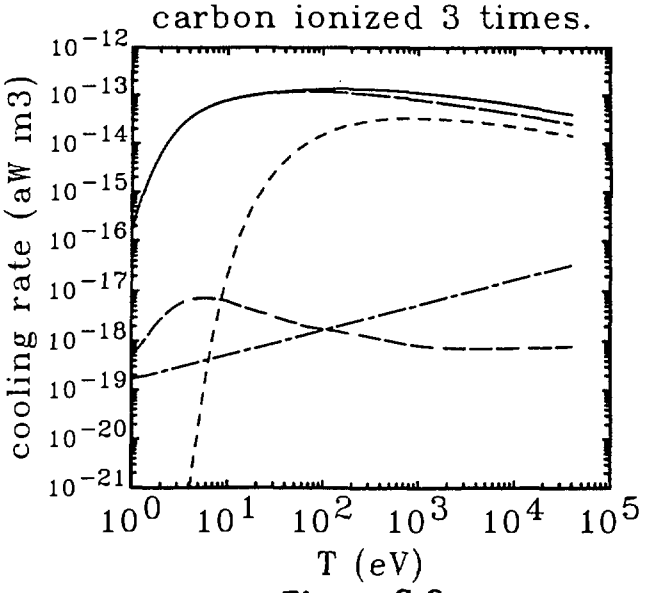

Figure C-8

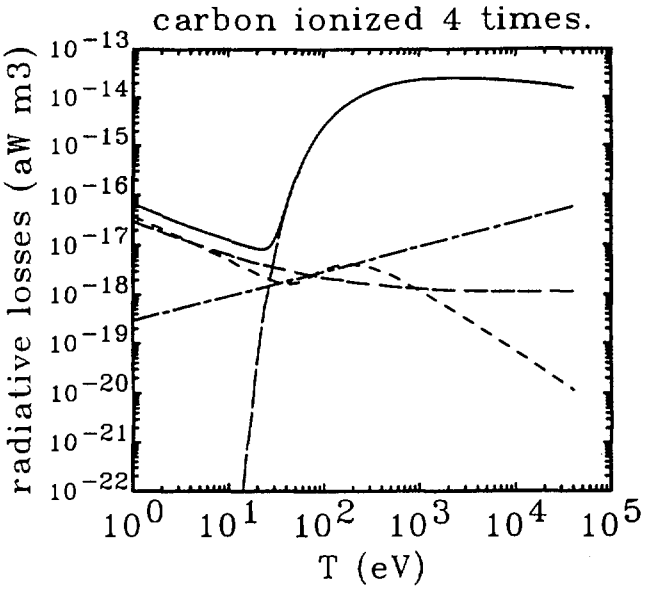

Figure C-9

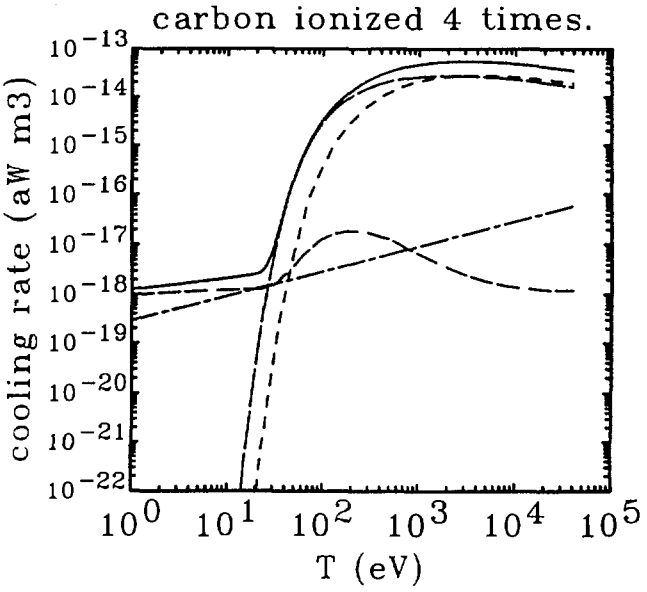

Figure C-10

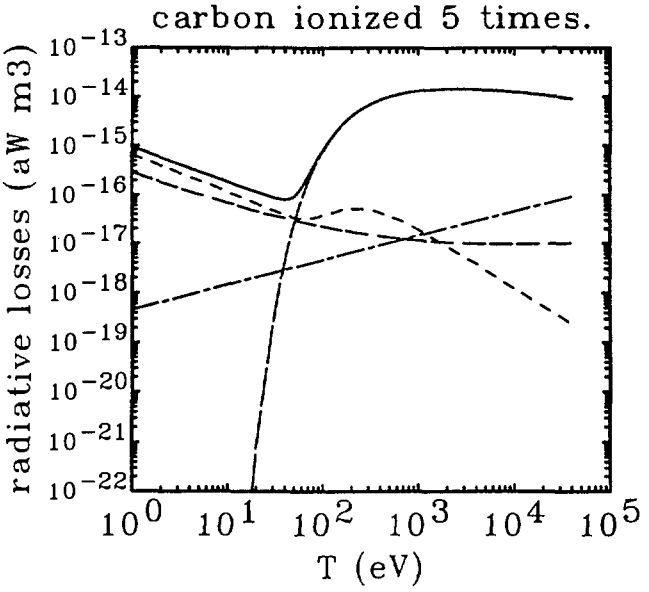

Figure C-11

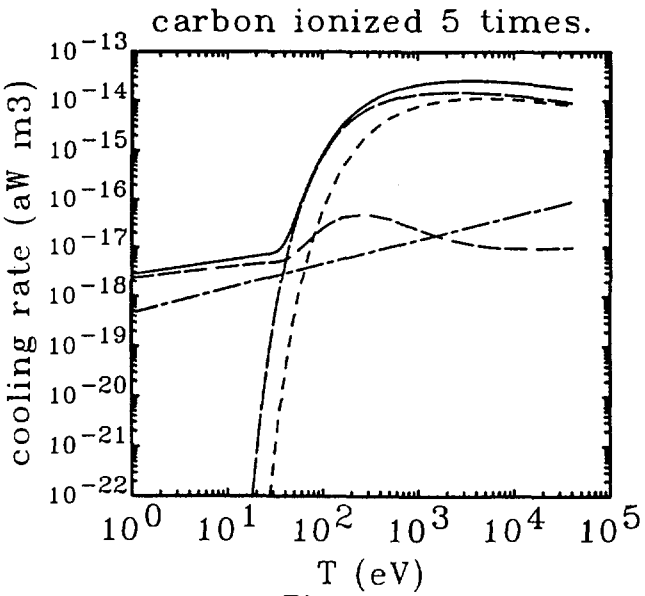

Figure C-12

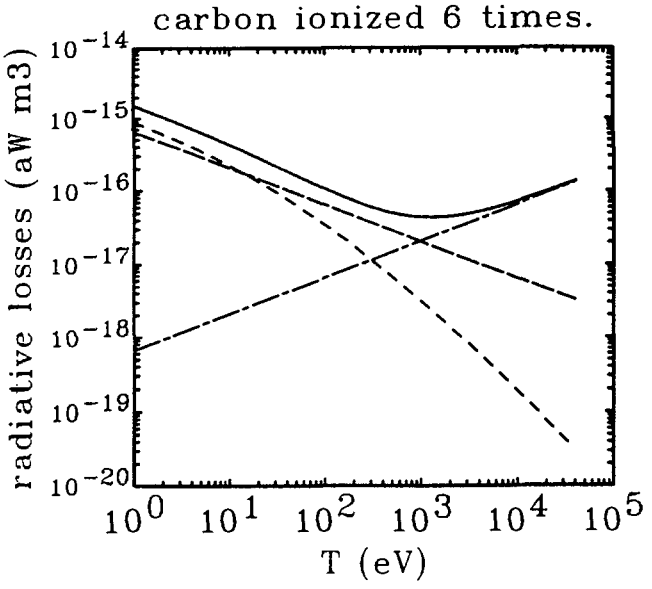

Figure C-13

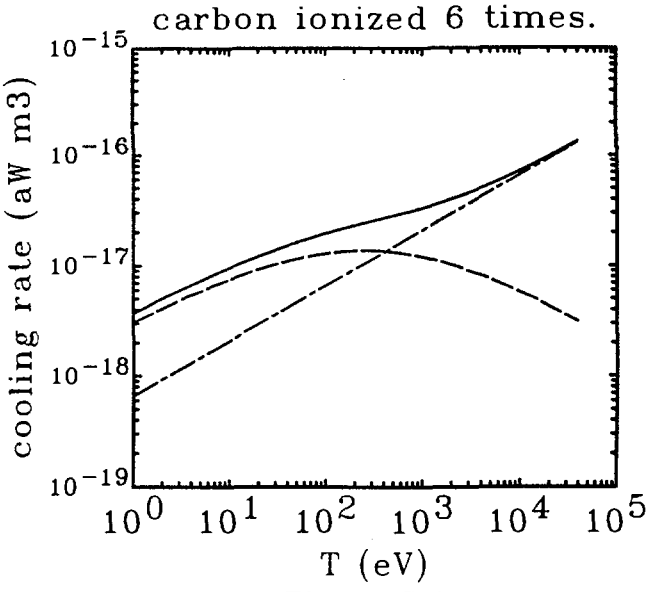

Figure C-14

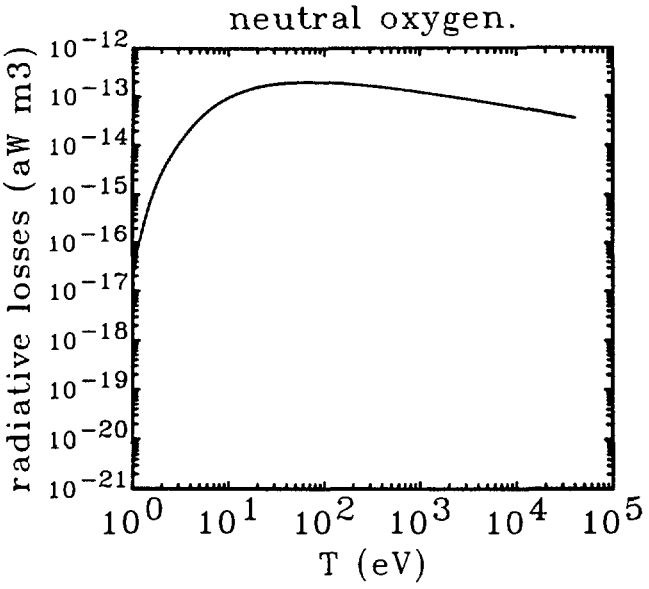

Figure C-15

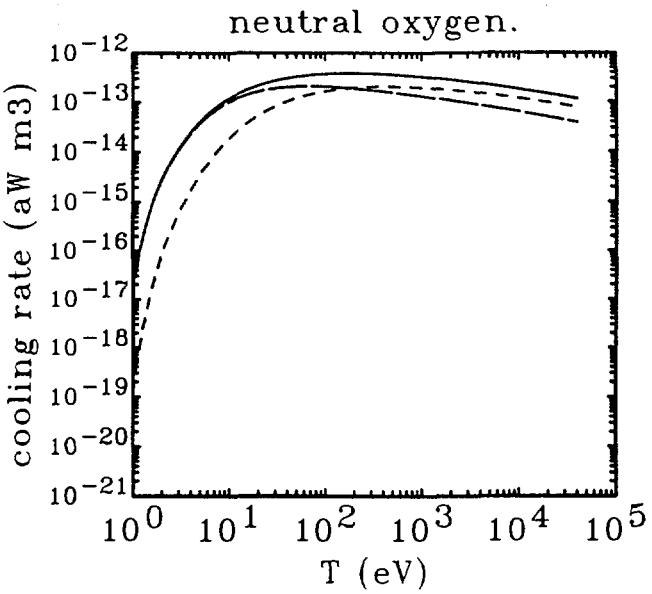

Figure C-16

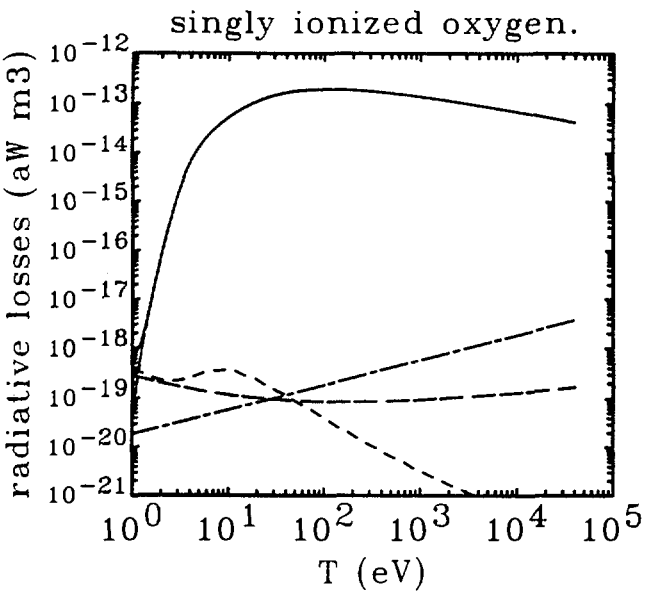

Figure C-17

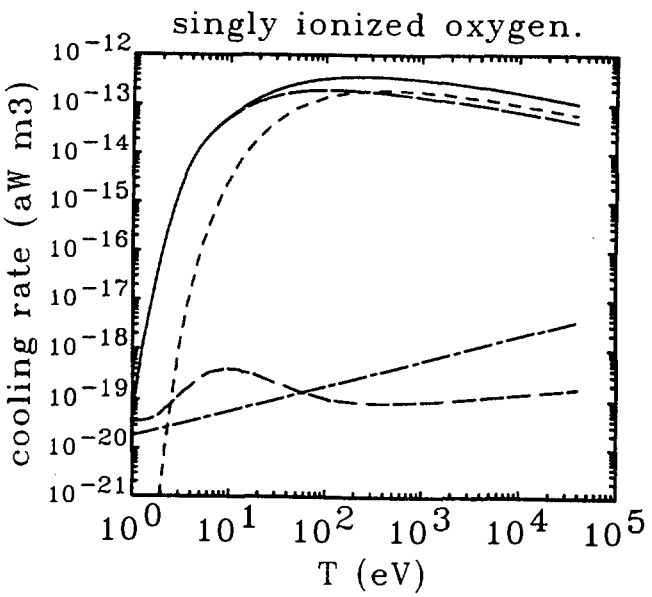

Figure C-18

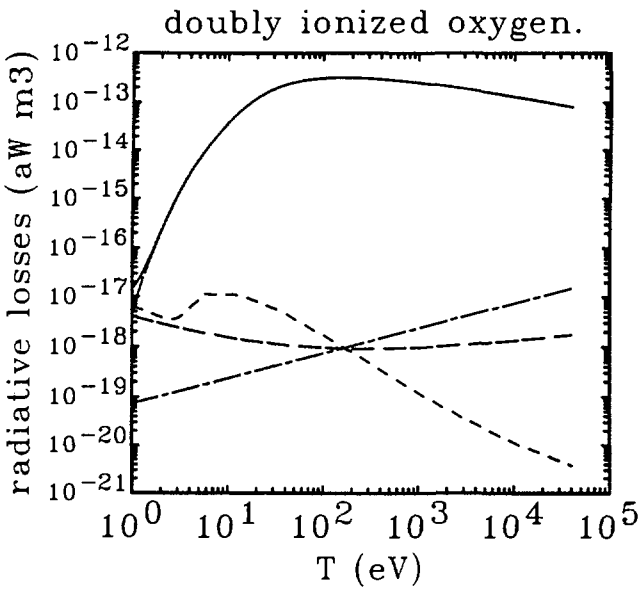

Figure C-19

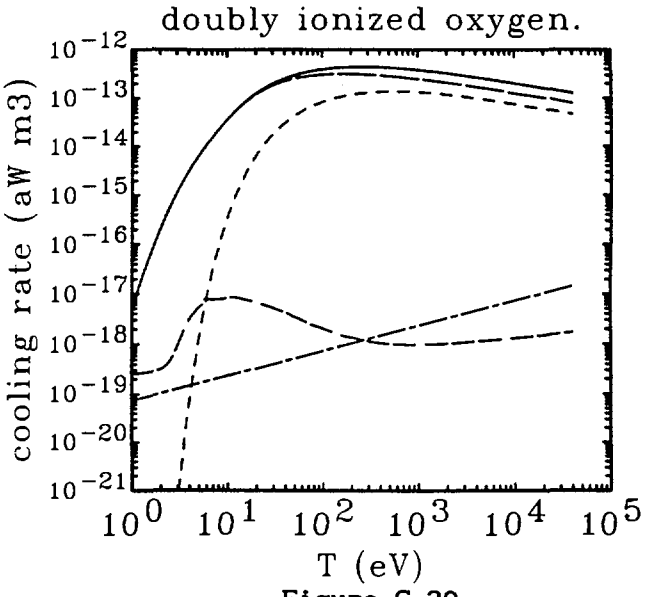

Figure C-20

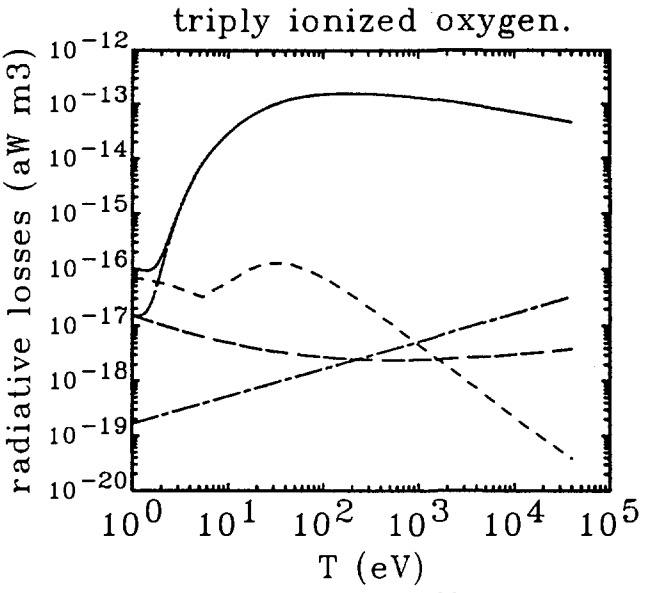

Figure C-21

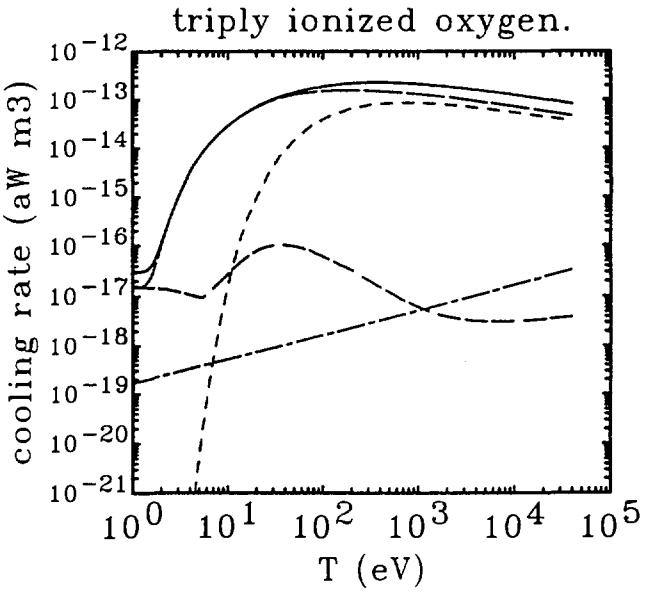

Figure C-22

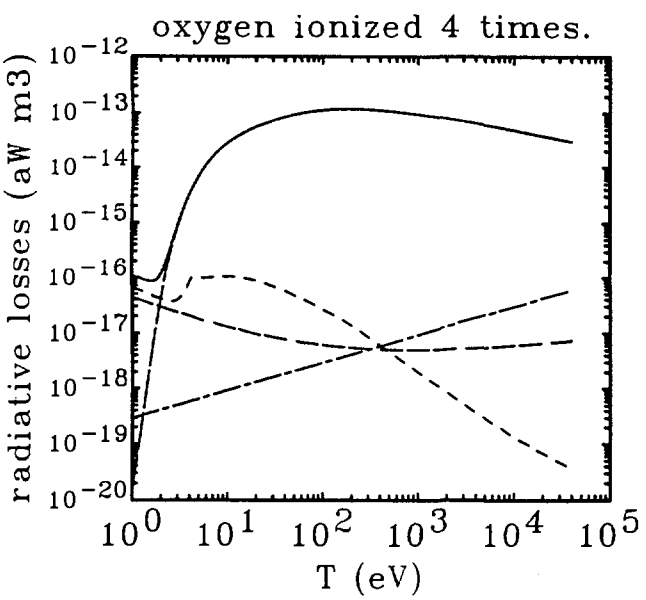

Figure C-23

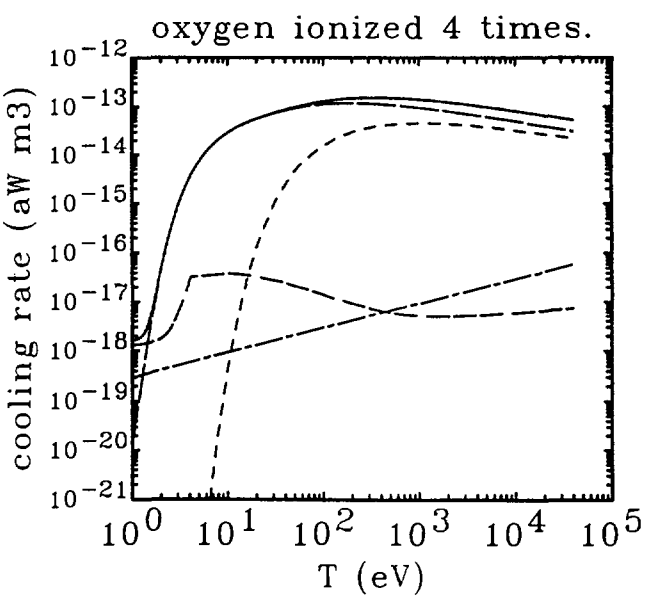

Figure C-24

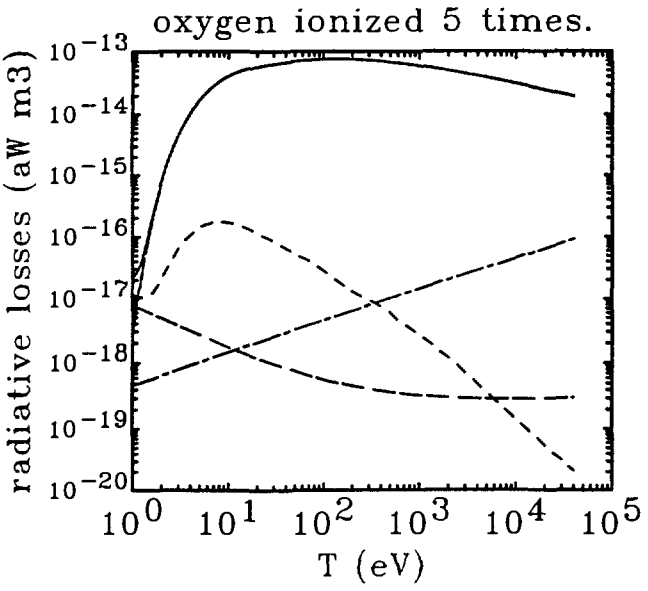

Figure C-25

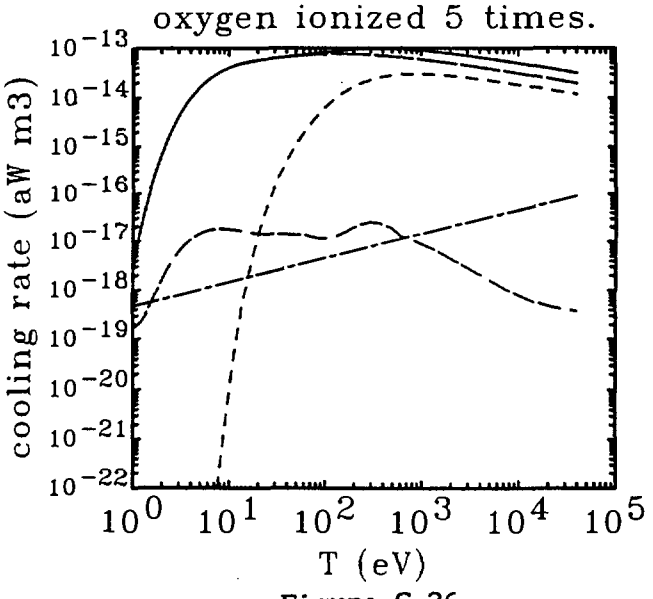

Figure C-26

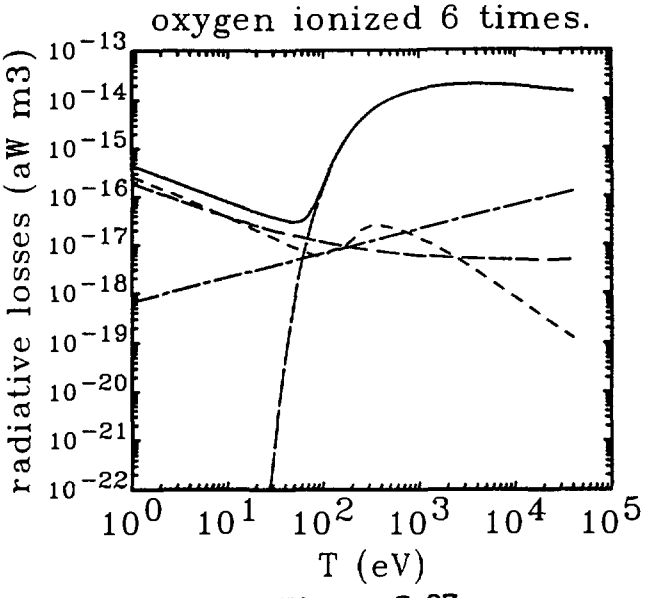

Figure C-27

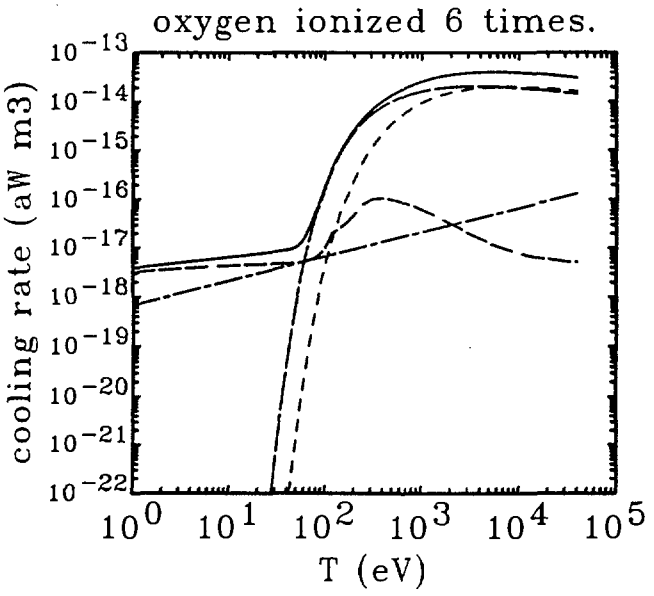

Figure C-28

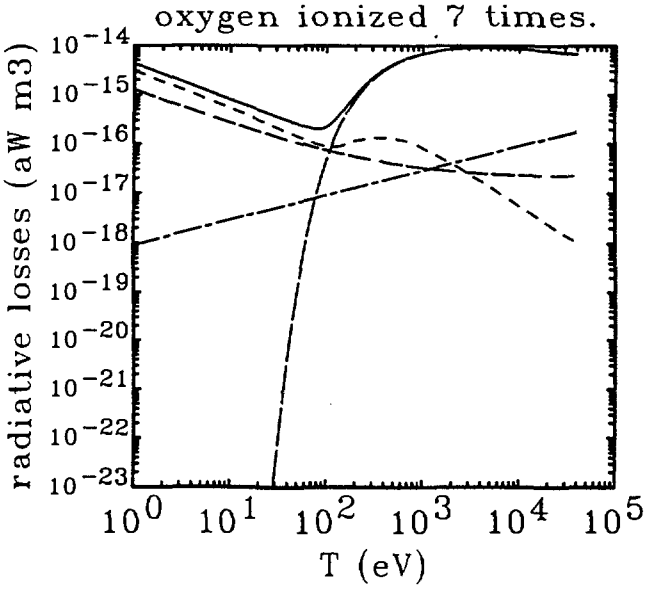

Figure C-29

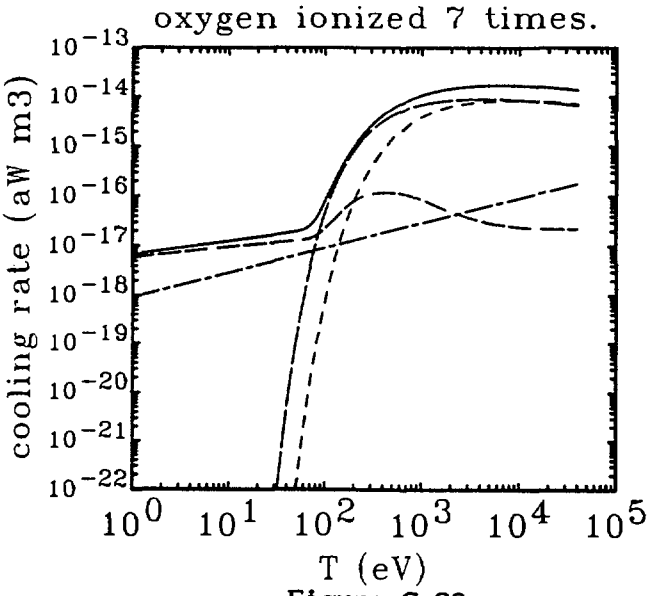

Figure C-30

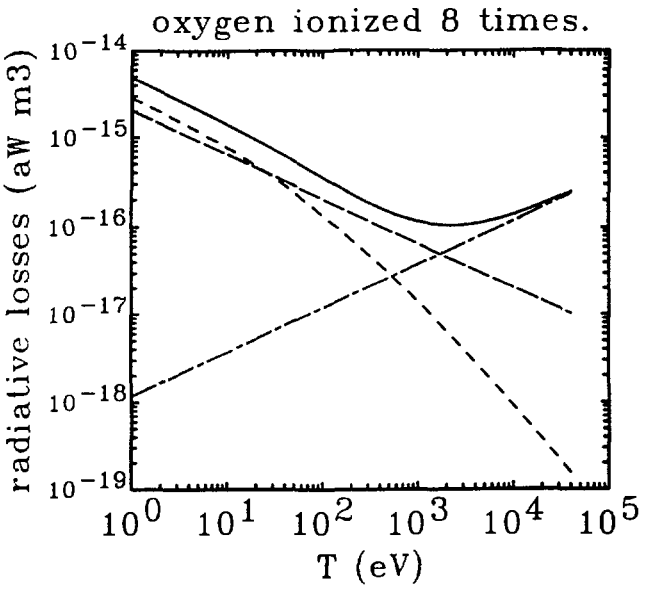

Figure C-31

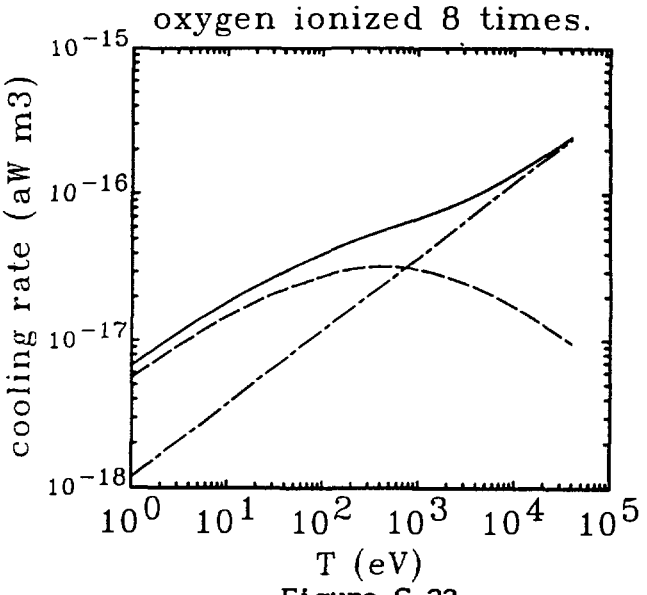

Figure C-32

Appendix D. Radiative losses and electron cooling rates calculated for carbon and oxygen at steady ionisation balance.

In this appendix we present the radiative and cooling rates computed for carbon and oxygen at steady ionisation balance. The method of calculation is that of Sec. 2.3.4, and the atomic data used are as described in Sec. 3. The various contributions considered for the radiative power loss and electron cooling rate functions are as described in Appendix C. The rates are given in units of attowatts m^3. We recall that 1 aW = 10^{-18}W. The results are given in the figures which follow.

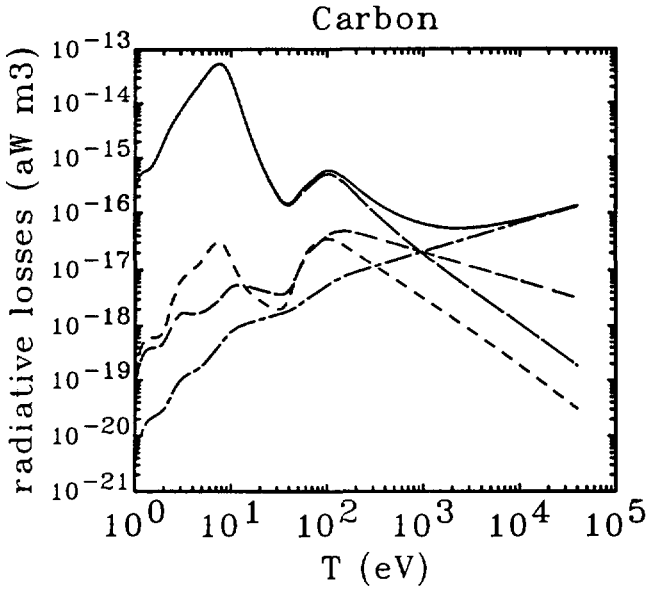

Figure D-1

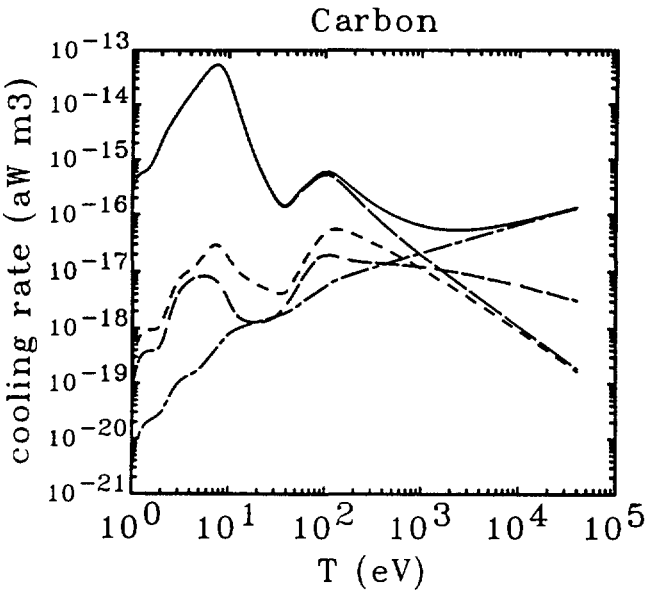

Figure D-2

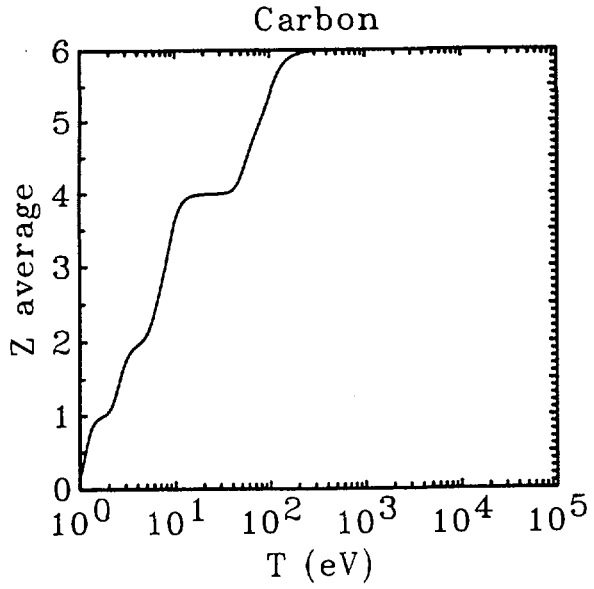

Figure D-3

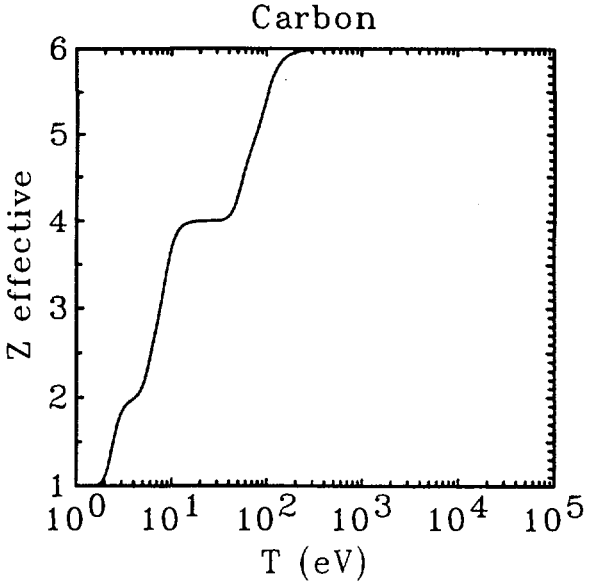

Figure D-4

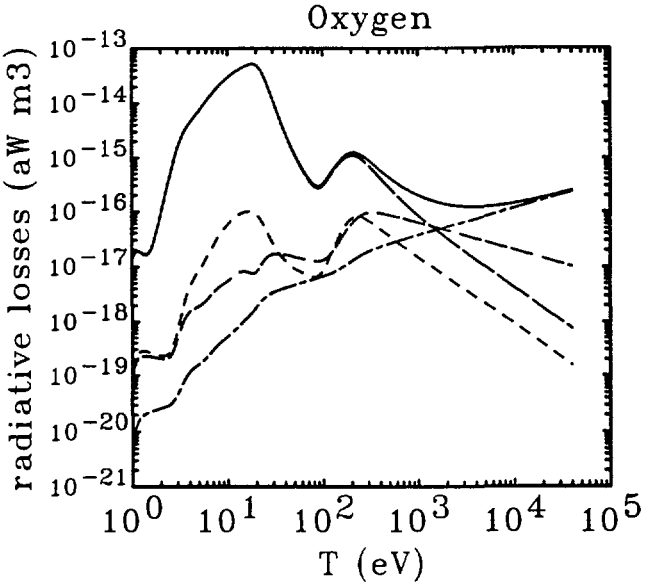

Figure D-5

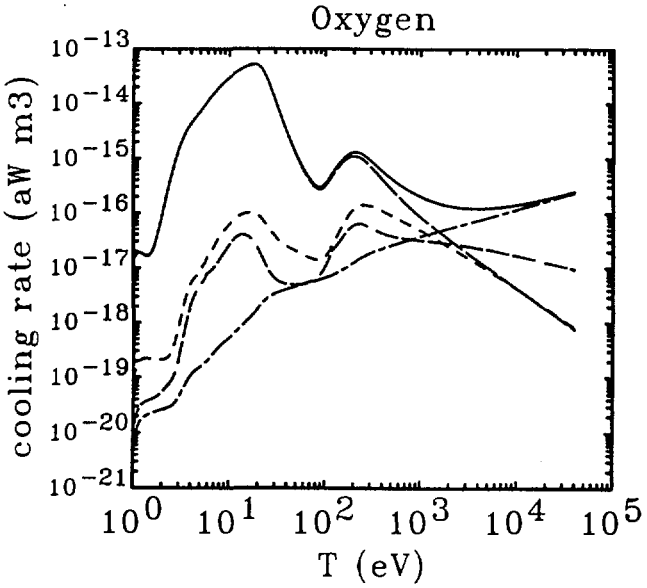

Figure D-6

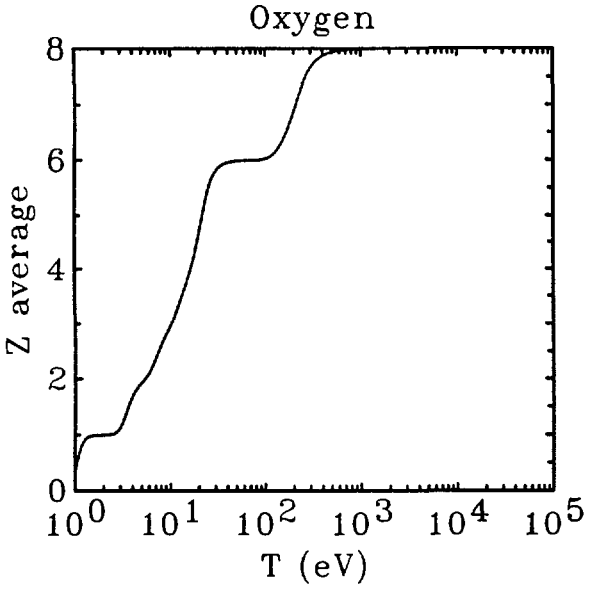

Figure D-7

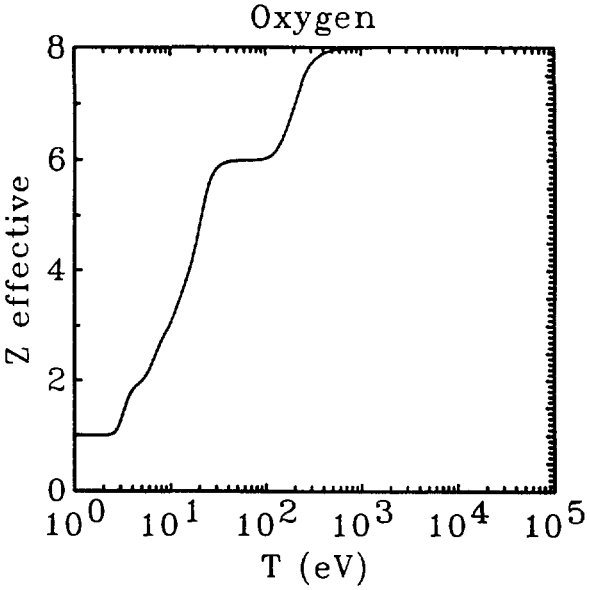

Figure D-8